





Deflection angle, quasinormal modes and optical properties of a de Sitter black hole in $f(\mathcal{T}, \mathcal{B})$ gravity

Nashiba Parbin ^{*}, Dhruba Jyoti Gogoi [†], Jyatsnasree Bora [‡] and Umananda Dev Goswami [§]
Department of Physics, Dibrugarh University, Dibrugarh 786004, Assam, India

The current study aims to examine the impact of the boundary term on the bending angle of light for a static spherically symmetric black hole in the modified gravity described by the $f(\mathcal{T}, \mathcal{B})$ function. To accomplish this objective, we employ the Ishihara *et al.* method, which enables us to compute the deflection angle of light for a receiver and source situated at finite distances from a lens object in a non-asymptotically flat spacetime. This method considers the receiver's viewpoint, and the resulting deflection angle diverges as the distance from the lens object increases, owing to the non-asymptotically flat spacetime. Nevertheless, the divergence can be regulated by the boundary term parameter c_0 . For lower values of the parameter c_0 , the divergence can be minimized within the finite range of the observer and source. Furthermore, we calculate the quasinormal modes of massless scalar perturbations in the black hole's background using the asymptotic iteration method (AIM) and Padé averaged sixth-order Wentzel-Kramers-Brillouin (WKB) approximation method. Our findings indicate that the real quasinormal modes and damping rates are significantly impacted by the model parameter c_0 . Subsequently, we investigate two optical characteristics of the black hole, namely the shadow and the emission rate. Our results show that with an increase in the boundary term parameter c_0 , both the shadow's size and the evaporation rate decrease.

PACS numbers:

Keywords: Modified gravity; Deflection angle; Quasinormal modes, Black hole shadow and emission rate

I. INTRODUCTION

The revolutionary idea of the theory of general relativity (GR) first struck in the great mind of Albert Einstein, which he published in 1915 [1]. After the time of publication of this theory, it has gained utmost importance in describing many gravitational phenomena. Among different predictions of GR, black holes and gravitational waves (GWs) are two most significant ones. However, it has shown some limitations while explaining the current accelerated expansion of the universe [2, 3] as well as the observed rotational dynamics of the galaxies [4–8]. GR needs some exotic stuff called dark energy and dark matter [9–14] in order to overcome its limitations. Thus, in order to represent the observed facts of the present universe, it can be conjectured that either the universe is filled with mysterious dark matter and dark energy, or a plausible modified theory of gravity (MTG) should be used such that it can explain the correct outcomes from observations. At present there are lots of proposed MTGs that are introduced to resolve unexplained issues of the universe [15–26].

The first experimental verification of GR was observed in 1919. It was the observation of the gravitational bending of light, during a solar eclipse [27] as per the prediction of GR. Moreover, from the interpretation of gravitational bending of light in the framework of geometrical optics of a lens, a key idea, the gravitational lensing has emerged [28–31]. It was in 1979, when the first instance of gravitationally lensed object, the double quasar Q0957 + 561A,B was identified for the first time [32]. In the modern observational cosmology for exploring the exoplanets and for measuring the distribution of dark matter and dark energy, an important parameter is the angle of gravitational bending of light. For different black holes, the gravitational lensing around them has been investigated in a plethora of articles. For the case of Schwarzschild black hole such investigation was carried out in the Ref. [33]. For black holes in presence of the cosmological constant the studies of such lensing are reported in Ref.s [34, 35]. Again, the gravitational lensing by the naked singularity and horizonless ultracompact objects are studied in the Ref.s [36, 37].

In 2008, an alternative method for the derivation of deflection angle of light in a spherically symmetric black hole, introduced by Gibbons and Werner, by implementing the Gauss-Bonnet theorem (GBT) [38, 39] was reported in the Ref. [40]. This method is found to be good to calculate the exact form of the deflection angle in the weak field limit for Schwarzschild black hole spacetime [40]. Quite a few studies show that this approach can be used to derive the deflection angle for different black hole solutions [41–52]. To obtain the deflection angle by a Kerr black hole the Gibbons-Werner method was then extended using

*Email: nashibaparbin91@gmail.com

†Email: moloydhruba@yahoo.in

‡Email: jyatsnasree.borah@gmail.com

§Email: umananda2@gmail.com

the Kerr-Randers optical geometry [53, 54]. This method was further extended in 2016 by Ishihara *et al.* to consider finite distances between the source and the observer for static as well as stationary black hole solutions [55]. For stationary black hole spacetimes, extension of this method is reported in the Ref.s [56–60]. For the case of asymptotically non-flat spacetimes such study can be found in the Ref.s [61–63]. Using different MTGs such studies on gravitational deflection angle using GBT are reported in [59, 63, 64]. Using GBT the effect of dark matter on deflection angle is also reported earlier in a few articles [65–68].

In our work, we intend to explore the impact of the modification of spacetime curvature on the gravitational lensing of a static spherically symmetric black hole spacetime. For this purpose, we consider the black hole solution in the $f(\mathcal{T}, \mathcal{B})$ modified gravity theory [69]. The $f(\mathcal{T}, \mathcal{B})$ modified gravity has been investigated in various aspects [70–75], but for the case of gravitational lensing, we study for the first time the effects of $f(\mathcal{T}, \mathcal{B})$ gravity on the deflection angle of light for a static spherically symmetric black hole using the GBT. Here we shall implement the Ishihara method for the asymptotically non-flat spacetime to obtain the deflection angle.

In this work we also study the quasinormal modes [76, 77] of the considered black hole spacetime. In general these are the modes of emission of GWs from compact and massive perturbed objects in the universe and are represented by some complex numbers [78–81]. The real part of these complex numbers is related to the emission frequency, while the imaginary part is related to the damping of quasinormal modes of GWs. In the last few years a number of authors have investigated the properties of GWs and also quasinormal modes of black holes in different MTGs [23, 82–91].

Furthermore, we analyze the effect that the modification of curvature has on the shadow cast by the black hole in $f(\mathcal{T}, \mathcal{B})$ gravity. The shadow is a characteristic feature of a black hole and is cast as a result of the strong gravitational field of the black hole. The shape and size of the shadow depend directly on the mass and angular momentum of the black hole. Studies on the shadow cast by a black hole have been of current interest to the scientific community [57, 59, 92–116, 118–133], more so after the successful release of the black hole images. The studies of the shadow cast by black holes surrounded by exotic dark matter have also been carried out in various literature [134–137]. Also, the analysis of the shadow cast by a black hole can aid in characterizing the various gravity theories [98]. Finally, we discuss and analyze the behaviour of the emission rate of particles around the black hole. It is another observable phenomena which has also gained interest and has been studied in literature [138–144].

Our paper is organized as follows. In Sec. II, we briefly review the field equations related to the $f(\mathcal{T}, \mathcal{B})$ modified gravity theory. In Sec. III, we derive the deflection angle in the spacetime of the static black hole in $f(\mathcal{T}, \mathcal{B})$ gravity applying Ishihara *et al.* method for asymptotically non-flat spacetime. The quasinormal modes of the black hole are studied in Sec. IV. In Sec. V, we have studied the optical properties, namely, the shadow and emission rate of the black hole. Finally, in Sec. VI, we summarize and conclude the results of our work. Throughout our work, we have imposed the sign convention $(-, +, +, +)$.

II. $f(\mathcal{T}, \mathcal{B})$ GRAVITY AND A STATIC SPHERICALLY SYMMETRIC BLACK HOLE SOLUTION

An alternative geometrical formulation of GR can be made through the teleparallel equivalent of general relativity (TEGR). In other words the TEGR is an analogous theory of GR as this theory asserts that GR can be formulated from the tetrad fields as well as from the torsion tensor [145, 146]. A generalization of the TEGR is the $f(\mathcal{T})$ gravity, a function of the torsion scalar \mathcal{T} , which is obtained by the contraction of the torsion tensor $\mathcal{T}^a{}_{\mu\nu}$ defined as [69, 146]

$$\mathcal{T}^a{}_{\mu\nu} = \partial_\mu h^a{}_\nu - \partial_\nu h^a{}_\mu, \quad (1)$$

where $h^a{}_\mu$ are the tetrad fields, related to the metric $g_{\mu\nu}$ via the Minkowski metric η_{ab} as

$$g_{\mu\nu} = h^a{}_\mu h^b{}_\nu \eta_{ab}. \quad (2)$$

A similar relationship between the inverse metric $g^{\mu\nu}$ and the inverse tetrads $h_a{}^\mu$ can be obtained. The conditions satisfied by the tetrads and the inverse tetrads are

$$h_b{}^\mu h^a{}_\mu = \delta_b^a, \quad h_a{}^\mu h^a{}_\nu = \delta_\nu^\mu. \quad (3)$$

A more generalization to the $f(\mathcal{T})$ gravity is done by introducing a boundary term \mathcal{B} related to the divergence of the torsion vector $\mathcal{T}_\mu = \mathcal{T}^\alpha{}_{\alpha\mu}$ as $\mathcal{B} = \frac{2}{h} \partial_\mu (h \mathcal{T}^\mu)$, where $h = \det(h^a{}_\mu) = \sqrt{-g}$ is the determinant of the tetrads $h^a{}_\mu$ with g being determinant of the metric $g_{\mu\nu}$. This theory was introduced in [69]. The action of the $f(\mathcal{T}, \mathcal{B})$ gravity is

$$S_{f(\mathcal{T}, \mathcal{B})} = \int d^4x h \left[\frac{1}{2\kappa^2} f(\mathcal{T}, \mathcal{B}) + \mathcal{L}_m \right], \quad (4)$$

with $\kappa^2 = 8\pi G$ and \mathcal{L}_m being the Lagrangian density of matter. The field equations of this theory can be obtained as [69, 74]

$$\begin{aligned} \delta_\nu^\lambda \overset{\circ}{\square} f_{\mathcal{B}} - \overset{\circ}{\nabla}^\lambda \overset{\circ}{\nabla}_\nu f_{\mathcal{B}} + \frac{1}{2} \mathcal{B} f_{\mathcal{B}} \delta_\nu^\lambda + [(\partial_\mu f_{\mathcal{B}}) + (\partial_\mu f_{\mathcal{T}})] S_\nu{}^{\mu\lambda} + h^{-1} h^a{}_\nu \partial_\mu (h S_a{}^{\mu\lambda}) f_{\mathcal{T}} \\ - f_{\mathcal{T}} \mathcal{T}^\sigma{}_{\mu\nu} S_\sigma{}^{\lambda\mu} - \frac{1}{2} f \delta_\nu^\lambda = \kappa^2 T_\nu^\lambda. \end{aligned} \quad (5)$$

In this expression the circle over the terms is used to denote the quantities which are determined using the Levi-Civita connection and the subscripts below the functional f denote the respective derivatives. The term T_ν^λ represents the energy-momentum tensor and the term $S_\nu^{\mu\lambda}$ is known as the superpotential tensor [74] defined as

$$S_\nu^{\mu\lambda} = K^{\mu\lambda}{}_\nu - \delta_\nu^\mu \mathcal{T}_\sigma^{\sigma\lambda} + \delta_\nu^\lambda \mathcal{T}_\sigma^{\sigma\mu} = -S_\nu^{\lambda\mu}, \quad (6)$$

where $K^\nu{}_{\mu\lambda}$ is the contortion tensor as given by

$$K^\nu{}_{\mu\lambda} = \Gamma^\nu{}_{\mu\lambda} - \overset{\circ}{\Gamma}{}^\nu{}_{\mu\lambda} = \frac{1}{2} (\mathcal{T}_\mu{}^\nu{}_\lambda + \mathcal{T}_\lambda{}^\nu{}_\mu - \mathcal{T}^\nu{}_{\mu\lambda}). \quad (7)$$

In Ref. [74] different exact and spherically symmetric perturbative solutions of field Eqs. (5) have been obtained. The black hole solution that we consider in our work is obtained by using the complex tetrad found in the Weitzenböck gauge ($\omega^A{}_{B\mu} = 0$) [147]. This complex tetrad has been uniquely derived in [74], and is given by

$$h_{(2)\mu}^A = \begin{pmatrix} 0 & iB(r) & 0 & 0 \\ iA(r) \sin \vartheta \cos \phi & 0 & -\chi r \sin \phi & -r\chi \sin \vartheta \cos \vartheta \cos \phi \\ iA(r) \sin \vartheta \cos \phi & 0 & \chi r \cos \phi & -r\chi \sin \vartheta \cos \vartheta \sin \phi \\ iA(r) \cos \vartheta & 0 & 0 & \chi r \sin^2 \vartheta \end{pmatrix}, \quad (\chi = \pm 1), \quad (8)$$

where, $A(r)$ and $B(r)$ are the metric elements for a spherically symmetric metric of the form

$$ds^2 = -A(r) dt^2 + B(r) dr^2 + r^2 d\Omega^2, \quad (9)$$

where $d\Omega^2 \equiv d\theta^2 + \sin^2\theta d\phi^2$.

Following the approach described in [74] and using the complex tetrad (8) in the field equations (5) of $f(\mathcal{T}, \mathcal{B})$ gravity theory, the symmetric field equations for the complex tetrad are obtained as

$$\begin{aligned} \kappa^2 \rho &= -\frac{1}{2} f + \frac{2f_{\mathcal{T}}(rBA' + A(B - rB'))}{r^2 AB^3} + \frac{f_{\mathcal{B}}(r(B(rA'' + 4A') - rA'B') + 2A(B - rB'))}{r^2 AB^3} \\ &+ \frac{B' f'_{\mathcal{B}}}{B^3} - \frac{f''_{\mathcal{B}}}{B^2} + \frac{2f'_{\mathcal{T}}}{rB^2}, \end{aligned} \quad (10)$$

$$\kappa^2 p_r = \frac{1}{2} f + \frac{(rA' + 2A)f'_{\mathcal{B}}}{rAB^2} - \frac{2f_{\mathcal{T}}(2rA' + A)}{r^2 AB^2} + \frac{f_{\mathcal{B}}(r(rA'B' - B(rA'' + 4A')) - 2A(B - rB'))}{r^2 AB^3}, \quad (11)$$

$$\begin{aligned} \kappa^2 p_l &= \frac{1}{2} f - \frac{(rA' + A)f'_{\mathcal{T}}}{rAB^2} + \frac{f_{\mathcal{B}}(r(rA'B' - B(rA'' + 4A')) - 2A(B - rB'))}{r^2 AB^3} \\ &+ \frac{f_{\mathcal{T}}(r(rA'B' - B(rA'' + 3A')) - A(B - rB' + B^3))}{r^2 AB^3} - \frac{B' f'_{\mathcal{B}}}{B^3} + \frac{f''_{\mathcal{B}}}{B^2}, \end{aligned} \quad (12)$$

where, the primes represent derivation with respect to the radial coordinate r , and ρ , p_r and p_l are the energy density, radial pressure and lateral pressure of the fluid respectively.

Again, as reported in [74], for a functional form of the type $f(\mathcal{T}, \mathcal{B}) = \kappa_1 \mathcal{T} + F(\mathcal{B})$, Eqs. (10), (11) and (12) were utilized to obtain

$$-\frac{\kappa_1(r(B(rA'' + A') - rA'B') + A(rB' + B^3 - B))}{r^2 AB^3} = 0. \quad (13)$$

Solving this equation led to the derivation of an exact solution which behaves as Schwarzschild-de Sitter black hole solution. This black hole solution is of our interest as we wish to study the phenomenon of gravitational lensing by a black hole and its quasinormal modes in $f(\mathcal{T}, \mathcal{B})$ gravity theory. The Schwarzschild-de Sitter black hole solution is obtained by considering $\kappa_1 = 1/2$ and relating the metric elements as $A(r) = 1/B(r) = f(r)$ and is given by

$$ds^2 = -f(r) dt^2 + \frac{dr^2}{f(r)} + r^2 d\Omega^2, \quad (14)$$

where, the metric co-efficient is obtained as

$$f(r) = 1 - \frac{2M}{r} - (\Lambda + c_0 M) r^2. \quad (15)$$

The functional form of the $f(\mathcal{T}, \mathcal{B})$ gravity model considered in this solution is [74]

$$f(\mathcal{T}, \mathcal{B}) = \frac{\mathcal{T}}{2} - \frac{8c_0}{3\sqrt{\mathcal{B} + 18(Mc_0 + \Lambda)}} - 3\Lambda. \quad (16)$$

This functional form of $f(\mathcal{T}, \mathcal{B})$ is motivated from the fact that it leads to the unique Schwarzschild-de Sitter solution (14). It can be obtained by choosing $\kappa_1 = 1/2$ in the generalized functional form $f(\mathcal{T}, \mathcal{B}) = \kappa_1\mathcal{T} + F(\mathcal{B})$, mentioned earlier, and deducing the remaining part of this relation, i.e. $F(\mathcal{B})$, by using Eq. (13) following the Ref. [74]. The solution for the term $F(\mathcal{B})$ is made in such a way that the model presented in Eq. (16) leads to the Schwarzschild-de Sitter solution (14) (see [74] for details). Here c_0 is a parameter of the model carrying the effect of the boundary term \mathcal{B} . It is a dimensional parameter having the dimension of Length^{-3} . Thus the solution is found to have an effective cosmological constant due to the contribution from the boundary term as given by $\Lambda_{eff} = \Lambda + c_0M$. One can estimate an observational limit on c_0 from the shadow of black holes. For example, considering the black hole metric (14), we can have an expression of the shadow of an asymptotically flat black hole for a static observer at large distance as given by (details are discussed in the Section V(A))

$$R_s = \frac{3M}{\sqrt{\frac{1}{3} - 9M^2(c_0M + \Lambda)}}. \quad (17)$$

Following Ref. [148] and considering M87* black hole shadow, it is possible to have the following cases,

$$c_0 \leq 1.11 \times 10^{-49} - 2.15 \times 10^{-21} \Lambda \text{ kpc}^{-3}, \quad (18)$$

and

$$c_0 \leq 1.59 \times 10^{-49} - 2.15 \times 10^{-21} \Lambda \text{ kpc}^{-3}. \quad (19)$$

Although the tetrad used for the derivation of the exact black hole solution is complex, however the torsion scalar \mathcal{T} and the boundary term \mathcal{B} are real, and eventually, for the black hole solution (14), the torsion scalar and the boundary term are obtained as

$$\mathcal{T} = \frac{4}{r^2} + (\Lambda + c_0M) \left(\frac{16M}{r} - 12 \right), \quad (20)$$

$$\mathcal{B} = \frac{4}{r^2} + (\Lambda + c_0M) \left(\frac{40M}{r} - 36 \right). \quad (21)$$

One important point to be noted here is that the black hole solution (14) is not asymptotically flat because of the presence of r^2 term in the last part of the metric function (15). In this work we shall use this black hole solution to study the gravitational deflection of light and the quasinormal modes as discussed in the following sections.

III. GRAVITATIONAL DEFLECTION OF LIGHT

We follow the Ishihara *et al.* approach [55] to obtain the deflection angle of light in the weak field limit of the non-asymptotically flat black hole spacetime given by the solution (14). Here, as shown in Fig. 1, the black hole works as a lens (L), which is at a finite distance from the source (S) and the receiver (R). In the equatorial plane ($\theta = \pi/2$), the deflection angle can be expressed as [55, 56]

$$\hat{\Theta} = \Psi_R - \Psi_S + \phi_{RS}, \quad (22)$$

where Ψ_R and Ψ_S are the angles of light that are measured with respect to the lens at the positions of the receiver and the source respectively. $\phi_{RS} = \phi_R - \phi_S$ is the separation angle between the receiver and the source. Here, ϕ_R and ϕ_S are the longitudes of the receiver and the source respectively.

Since the light rays follow the null geodesic for which $ds^2 = 0$, the metric Eq. (14) can be rewritten for this geodesic as

$$dt^2 = \gamma_{ij} dx^i dx^j = \frac{1}{f(r)^2} dr^2 + \frac{r^2}{f(r)} d\Omega^2, \quad (23)$$

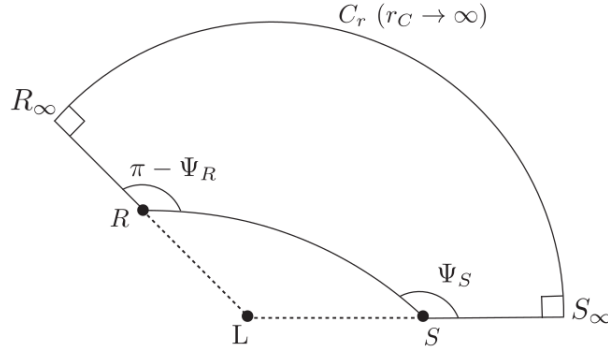


FIG. 1: Schematic figure for the quadrilateral $\overset{\infty}{R}\square\overset{\infty}{S}$ embedded in a curved space [62].

where γ_{ij} is usually known as the optical metric, which specifies a 3D Riemannian space. We will denote this space by $\mathcal{M}^{(3)}$, where a ray of light is considered as a spatial curve. By using the optical metric γ_{ij} , we can define the angles Ψ_R and Ψ_S . The non-vanishing components of this metric are

$$\gamma_{rr} = \frac{1}{f(r)^2}, \quad \gamma_{\phi\phi} = \frac{r^2}{f(r)}. \quad (24)$$

An important parameter in the study of gravitational deflection angle of light is the impact parameter of light in the black hole spacetime. This is usually defined as the ratio of the angular momentum (L) to the energy (\mathcal{E}) of photons, which are the constant of motion in the equatorial plane of spacetime. For the spacetime of black hole (14) these two constants of motion are $\mathcal{E} = f(r) \dot{t}$ and $L = r^2 \dot{\phi}$, where the over dot denotes the derivative with respect to the affine parameter λ along the path of the light ray. Thus the impact parameter of a light ray is

$$\xi \equiv \frac{L}{\mathcal{E}} = \frac{r^2}{f(r)} \frac{d\phi}{dt}. \quad (25)$$

The unit radial vector from the center of the lens can be obtained as $e_{rad} = (f(r), 0)$, and the unit angular vector along the angular direction can be found as $e_{ang} = (0, f(r)/r)$. Again, the components of the unit tangent vector $\mathbf{K} \equiv dx/dt$ along the light ray are obtained as [55]

$$(K^r, K^\phi) = \frac{\xi f(r)}{r^2} \left(\frac{dr}{d\phi}, 1 \right). \quad (26)$$

Here $dr/d\phi$ gives the orbital path variation of the rays of light known as the orbit equation, which can be expressed as

$$\left(\frac{dr}{d\phi} \right)^2 = -r^2 f(r) + \frac{r^4}{\xi^2}. \quad (27)$$

Now, if Ψ denotes the angle between the radial component of the tangent vector and the radial vector, i.e. the angle of the light ray which is measured from the radial direction, then we can write,

$$\cos \Psi = \frac{\xi}{r^2} \frac{dr}{d\phi}. \quad (28)$$

It gives,

$$\sin \Psi = \frac{\xi \sqrt{f(r)}}{r}. \quad (29)$$

Moreover, in a general form Eq. (27) can be expressed as

$$\left(\frac{du}{d\phi} \right)^2 = F(u), \quad (30)$$

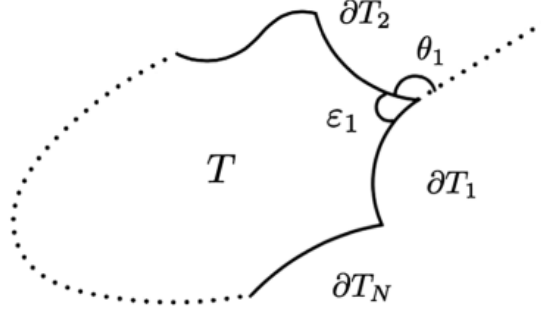


FIG. 2: Schematic figure for Gauss-Bonnet theorem [55]. The inner angle is ε_a and the jump angle is θ_a ($a = 1, 2, \dots, N$).

where we have considered a new variable $u = 1/r$ and hence the function $F(u) = -u^2 f(u) + 1/\xi^2$.

As mentioned earlier, we will use the GBT to calculate the deflection angle $\hat{\Theta}$. The GBT has many formulations. The simplest one states that the total Gaussian curvature of an embedded triangle can be expressed in terms of the total geodesic curvature of the boundary and the jump angles at the corners. Thus, mathematically this simplest version of the GBT can be expressed as [38]

$$\iint_T \mathcal{K} dS + \sum_{a=1}^N \int_{\partial T_a} \kappa_g dl + \sum_{a=1}^N \theta_a = 2\pi, \quad (31)$$

where T is a two-dimensional orientable surface shown in Fig. 2. The boundaries of the surface ∂T_a ($a = 1, 2, \dots, N$) are differentiable curves. θ_a are the jump angles between the curves. \mathcal{K} is the Gaussian curvature of the orientable surface T , κ_g is the geodesic curvature of ∂T_a , dS is the infinitesimal area element of the surface and dl is the infinitesimal line element along the boundary. Also, $dl > 0$ for prograde motion of photons and for retrograde motion $dl < 0$. The sign of dl is chosen to be consistent with the orientation of the surface T .

At this stage, we should note that the quadrilateral $\overset{\infty}{R}\square\overset{\infty}{S}$ shown in Fig. 1 is embedded in a curved space $\mathcal{M}^{(3)}$ and consists of a spatial curve for a light ray from the source to the receiver, two outgoing radial lines from R and from S , and a circular arc segment C_r with the coordinate radius r_C ($r_C \rightarrow \infty$). As clear from the figure, within the asymptotically flat spacetime, $\kappa_g \rightarrow 1/r_C$ and $dl \rightarrow r_C d\phi$ as $r_C \rightarrow \infty$ [40]. Hence, the deflection angle can be defined in the domain $\overset{\infty}{R}\square\overset{\infty}{S}$ as

$$\hat{\Theta} = \Psi_R - \Psi_S + \phi_{RS} = - \int \int_{\overset{\infty}{R}\square\overset{\infty}{S}} \mathcal{K} dS \quad (32)$$

The separation angle ϕ_{RS} for our system can be obtained by integrating Eq. (30) as given by

$$\phi_{RS} = 2 \int_0^{u_0} \frac{du}{\sqrt{F(u)}}, \quad (33)$$

where u_0 is the inverse of the distance of closest approach. As in the Ishihara *et al.* method, if we consider that the source and the receiver are at finite distances from each other, then deflection angle can be written as

$$\hat{\Theta} = \Psi_R - \Psi_S + \int_{u_R}^{u_0} \frac{du}{\sqrt{F(u)}} + \int_{u_S}^{u_0} \frac{du}{\sqrt{F(u)}}. \quad (34)$$

Again, for the metric (14) using Eq. (29), we obtain,

$$\begin{aligned} \Psi_R - \Psi_S = & \arcsin(\xi u_R) + \arcsin(\xi u_S) - \pi + \frac{\xi(\Lambda + c_0 M)}{2} \left[\frac{u_R^{-1}}{\sqrt{1 - \xi^2 u_R^2}} + \frac{u_S^{-1}}{\sqrt{1 - \xi^2 u_S^2}} \right] + \xi M \left[\frac{u_R}{\sqrt{1 - \xi^2 u_R^2}} \right. \\ & \left. + \frac{u_S}{\sqrt{1 - \xi^2 u_S^2}} \right] + \frac{\xi M \Lambda}{2} \left[\frac{1 - 2\xi^2 u_R^2}{(1 - \xi^2 u_R^2)^{3/2}} + \frac{1 - 2\xi^2 u_S^2}{(1 - \xi^2 u_S^2)^{3/2}} \right] + \frac{\xi M c_0 \Lambda}{4} \left[\frac{u_R^{-3}}{(1 - \xi^2 u_R^2)^{3/2}} + \frac{u_S^{-3}}{(1 - \xi^2 u_S^2)^{3/2}} \right] \\ & - \frac{\xi^3 M c_0 \Lambda}{2} \left[\frac{u_R^{-1}}{(1 - \xi^2 u_R^2)^{3/2}} + \frac{u_S^{-1}}{(1 - \xi^2 u_S^2)^{3/2}} \right] + \mathcal{O}(M^2, M\Lambda^2, \Lambda^2). \end{aligned} \quad (35)$$

Here, it can be seen that the expansion of $\Psi_R - \Psi_S$ becomes divergent at $u_R \rightarrow 0$ and $u_S \rightarrow 0$ due to the fact that our spacetime is non-asymptotically flat. Hence, this series Eq. (35) must be used only within a certain limit of finite radius of convergence. Moreover, for the metric (14) the function $F(u)$ can be expressed as

$$F(u) = \frac{1}{\xi^2} - u^2 + 2Mu^3 + (\Lambda + c_0M). \quad (36)$$

Hence, the angle ϕ_{RS} for the metric (14) is obtained as

$$\begin{aligned} \phi_{RS} = & \pi - \arcsin(\xi u_R) - \arcsin(\xi u_S) + \frac{M}{\xi} \left[\frac{2 - \xi^2 u_R^2}{\sqrt{1 - \xi^2 u_R^2}} + \frac{2 - \xi^2 u_S^2}{\sqrt{1 - \xi^2 u_S^2}} \right] \\ & + \frac{\xi^3(\Lambda + c_0M)}{2} \left[\frac{u_R}{\sqrt{1 - \xi^2 u_R^2}} + \frac{u_S}{\sqrt{1 - \xi^2 u_S^2}} \right] + \frac{\Lambda \xi M}{2} \left[\frac{2 - 3\xi^2 u_R^2}{(1 - \xi^2 u_R^2)^{3/2}} + \frac{2 - 3\xi^2 u_S^2}{(1 - \xi^2 u_S^2)^{3/2}} \right] \\ & - \frac{\Lambda \xi^5 c_0 M}{4} \left[\frac{3u_R - 2\xi^2 u_R^3}{(1 - \xi^2 u_R^2)^{3/2}} + \frac{3u_S - 2\xi^2 u_S^3}{(1 - \xi^2 u_S^2)^{3/2}} \right] + \mathcal{O}(M^2, M\Lambda^2, \Lambda^2). \end{aligned} \quad (37)$$

Using Eqs. (35) and (37), we finally get the deflection angle of light for our considered black hole as

$$\begin{aligned} \hat{\Theta} = & \frac{\xi(\Lambda + c_0M)}{2} \left[\frac{1 + \xi^2 u_R^2}{u_R \sqrt{1 - \xi^2 u_R^2}} + \frac{1 + \xi^2 u_S^2}{u_S \sqrt{1 - \xi^2 u_S^2}} \right] + \xi M \left[\frac{u_R}{\sqrt{1 - \xi^2 u_R^2}} + \frac{u_S}{\sqrt{1 - \xi^2 u_S^2}} \right] \\ & + \frac{\xi M \Lambda}{2} \left[\frac{3 - 5\xi^2 u_R^2}{(1 - \xi^2 u_R^2)^{3/2}} + \frac{3 - 5\xi^2 u_S^2}{(1 - \xi^2 u_S^2)^{3/2}} \right] + \frac{\xi c_0 M \Lambda}{4} \left[\frac{u_R^{-3}}{(1 - \xi^2 u_R^2)^{3/2}} + \frac{u_S^{-3}}{(1 - \xi^2 u_S^2)^{3/2}} \right] \\ & - \frac{\xi^3 c_0 M \Lambda}{2} \left[\frac{u_R^{-1}}{(1 - \xi^2 u_R^2)^{3/2}} + \frac{u_S^{-1}}{(1 - \xi^2 u_S^2)^{3/2}} \right] + \frac{M}{\xi} \left[\frac{2 - \xi^2 u_R^2}{\sqrt{1 - \xi^2 u_R^2}} + \frac{2 - \xi^2 u_S^2}{\sqrt{1 - \xi^2 u_S^2}} \right] \\ & - \frac{\xi^5 c_0 M \Lambda}{4} \left[\frac{3u_R - 2\xi^2 u_R^3}{(1 - \xi^2 u_R^2)^{3/2}} + \frac{3u_S - 2\xi^2 u_S^3}{(1 - \xi^2 u_S^2)^{3/2}} \right] + \mathcal{O}(M^2, M\Lambda^2, \Lambda^2). \end{aligned} \quad (38)$$

By virtue of Eq. (35) few terms in the above expression may diverge in the far distance limit, $u_R \rightarrow 0$, $u_S \rightarrow 0$. As mentioned earlier, this is due to the reason that the spacetime we have considered here is non-asymptotically flat, similar to the Kottler spacetime [149] used by Ishihara *et al.* [55]. As discussed in [55], we can state that this divergence in the deflection angle in the far distance limit does not matter as the limit $u_R \rightarrow 0$, $u_S \rightarrow 0$ is not applicable for astronomical observations. Also, the effect of the boundary term contribution $\Lambda_{eff} = \Lambda + c_0M$ on the deflection angle can be seen in Eq. (38). It is observed that the deflection angle will increase with an increase in the effective cosmological constant term. Thus, the boundary term coming from $f(\mathcal{T}, \mathcal{B})$ gravity has significant effect on the deflection angle. Further, from Eq. (38) for $\Lambda = c_0 = 0$, we can arrive at

$$\hat{\Theta} \simeq \frac{M}{\xi} \left[\frac{2 - \xi^2 u_R^2}{\sqrt{1 - \xi^2 u_R^2}} + \frac{2 - \xi^2 u_S^2}{\sqrt{1 - \xi^2 u_S^2}} \right], \quad (39)$$

which at the far distance limit ($u_R \rightarrow 0$, $u_S \rightarrow 0$), reduces to the deflection angle in the Schwarzschild case,

$$\hat{\Theta} \simeq \frac{4M}{\xi}. \quad (40)$$

Now, as an example we will explore the deflection angle for M87*, the central black hole candidate of M87 [150, 151] in the light of the above analysis. For this purpose we consider different values of the distance from the source r_s and also different values of the model parameter c_0 . The mass of this black hole is $\sim 6.5 \times 10^9 M_\odot \sim 10^{13}$ m. The distance of the receiver from M87* is its distance from the earth, which is ~ 16 Mpc $\sim 10^{23}$ m, and the recent cosmological data suggest the cosmological constant to be equal to $\Lambda = 10^{-52} \text{ m}^{-2}$ [152]. In Fig. 3, we plot the deflection angle as a function of the impact parameter, and compare our results with that of the Schwarzschild case. In the first panel of this figure, we have chosen a particular value of $r_s = 1$ Mpc. In this plot the solid curves depict the behaviour of the deflection angle for three positive values of the model parameter $c_0 = 0.01, 0.001, 0.0001$ and the dashed curves show the same for three negative values of the model parameter $c_0 = -0.0001, -0.001, -0.01$. All values of c_0 in this and rest of the calculations are used in the unit of kpc^{-3} . It can be seen that for $c_0 = 0.01$, the deflection angle decreases upto a certain value of the impact parameter and then abruptly increases. As the value of c_0 decreases, the deflection angle decreases with the impact parameter and increases slowly after a certain point. For $c_0 = 0.0001$, the curve almost overlaps with the Schwarzschild case upto a certain value of the impact parameter and then slowly

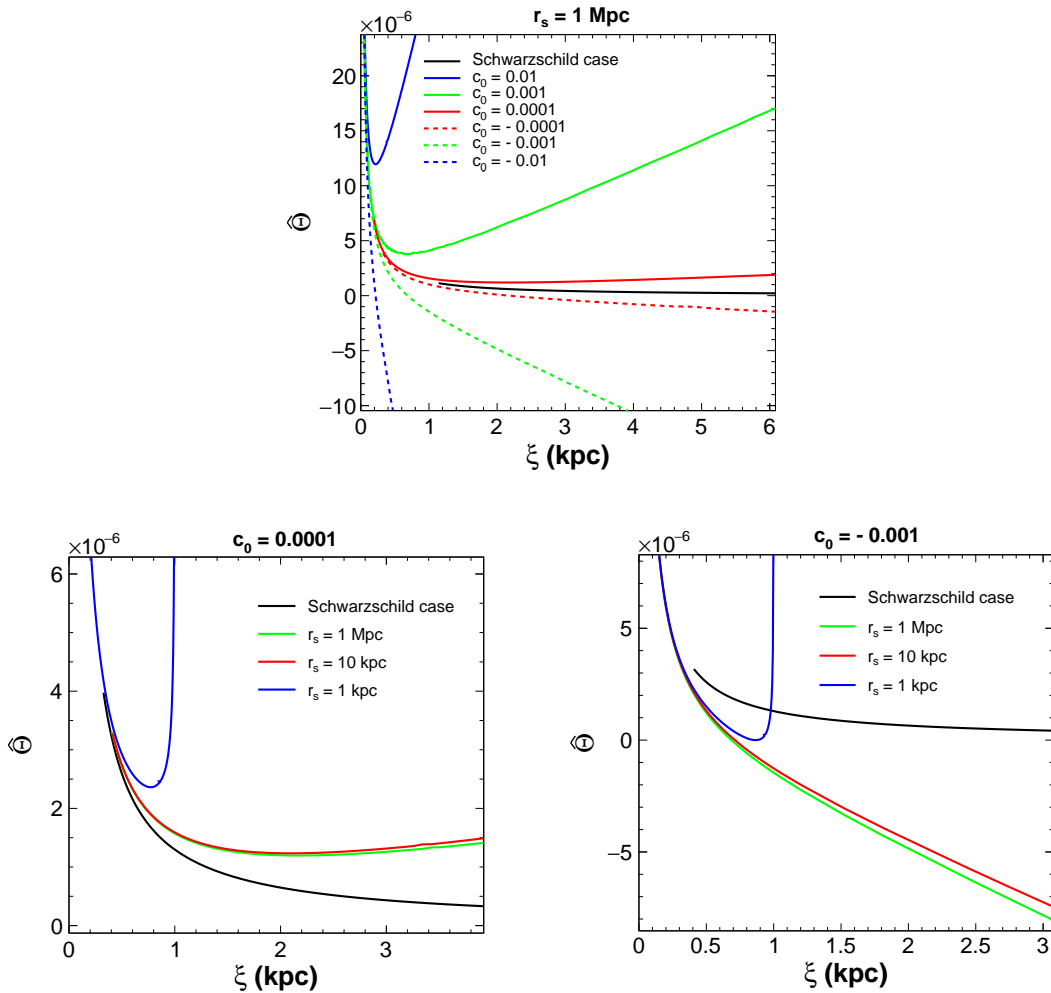


FIG. 3: Deflection angle as a function of impact parameter for the case of M87* black hole. In the first panel, we have considered $r_s = 1$ Mpc with three positive values of $c_0 = 0.01, 0.001, 0.0001$ in unit of kpc^{-3} which are shown by the solid curves, and three negative values of $c_0 = -0.0001, -0.001, -0.01$ in the same unit which are represented by the dashed curves. In the second and the last panel, we have chosen $r_s = 1$ Mpc, 10 kpc, 1 kpc with $c_0 = 0.0001 \text{ kpc}^{-3}$ and $c_0 = -0.001 \text{ kpc}^{-3}$ respectively.

increases. For the negative values of the model parameter, it is seen that the deflection angle decreases and becomes negative for a certain value of the impact parameter. For $c_0 = -0.0001$, the curve almost overlaps with the Schwarzschild case and then slowly becomes negative. This negative deflection angle signifies the behaviour of light around the black hole considered in our study. It can be said from our results that at certain impact parameter values, for $c_0 < 0$ cases, the photons get repelled leading to negative deflection of light. This can be comprehended as the repulsive gravitational effect of the teleparallel gravity theory [153, 154]. This type of negative deflection angle has been found in various studies [155–160]. In the second and the last panel, we plot the deflection angle as a function of the impact parameter for $c_0 = 0.0001$ and $c_0 = -0.001$ respectively, with three values of the distance from the source $r_s = 1$ Mpc, 10 kpc, 1 kpc. It is seen that if the source (say, a cluster of galaxies) is at a distance of 1 kpc, the deflection angle decreases till a certain point and then abruptly diverges for both the cases of $c_0 = 0.0001$ and $c_0 = -0.001$. However, for $c_0 = 0.0001$ the divergent behaviour is seen at a higher deflection angle than for $c_0 = -0.001$. If we consider a galaxy cluster further away, say at 10 kpc, there is a change in the way the deflection angle diverges for $c_0 = 0.0001$. Upto a certain value of the impact parameter, the deflection angle decreases in a way similar to the Schwarzschild case, but slowly becomes divergent after a particular value of the impact parameter. On the other hand, for $c_0 = -0.001$, the deflection angle decreases and eventually becomes negative after a certain value of the impact parameter. For both the values of c_0 , such similarities are also seen if we consider a cluster of galaxies at a distance of 1 Mpc. Thus, the divergent behaviour of the deflection angle is observed at low impact parameter value when the galaxy cluster is nearer to the lens.

IV. QUASINORMAL MODES

In this section, we will address the massless scalar perturbation in the spacetime of the black hole. We will assume that the test field exerts negligible influence on the black hole spacetime. To determine the quasinormal modes, we will derive Schrödinger-like wave equations taking into account the corresponding conservation relations of the concerned spacetime, which should be of Klein-Gordon type for the case of a scalar field. Two different methods, viz. the asymptotic iteration method (AIM) and the Padé averaged 6th order WKB approximation method, will be used to calculate the quasinormal modes. In this regard considering only the axial perturbations, we can express the perturbed metric as presented in [161]:

$$ds^2 = -|g_{tt}| dt^2 + r^2 \sin^2\theta (d\phi - p_1 dt - p_2 dr - p_3 d\theta)^2 + g_{rr} dr^2 + r^2 d\theta^2, \quad (41)$$

where p_1 , p_2 and p_3 define the perturbation introduced to the black hole spacetime and are functions of t , r and θ . The metric functions g_{tt} and g_{rr} represent the zeroth order terms and hence are only functions of r .

A. Scalar Perturbation

We consider a massless scalar field near the previously established black hole. As it is considered that the effect of scalar field on the black hole spacetime is minimal, the perturbed metric Eq. (41) in this case can be expressed as

$$ds^2 = -|g_{tt}| dt^2 + g_{rr} dr^2 + r^2 d\Omega^2. \quad (42)$$

Now, for this case, it is feasible to write the Klein-Gordon equation in curved spacetime as

$$\square\Phi = \frac{1}{\sqrt{-g}}\partial_\mu(\sqrt{-g}g^{\mu\nu}\partial_\nu\Phi) = 0. \quad (43)$$

With the help of this Eq. (43) the quasinormal modes associated with the scalar perturbation can be described. For this purpose we decompose the scalar field Φ as follows:

$$\Phi(t, r, \theta, \phi) = \frac{1}{r} \sum_{l,m} \psi_l(t, r) Y_{lm}(\theta, \phi). \quad (44)$$

In this equation, Y_{lm} is the spherical harmonics with l and m are the usual indices associated with it, $\psi_l(t, r)$ is the radial time-dependent wave function. Using Eqs. (43) and (44) one can obtain the radial wave equation as

$$\partial_{r_*}^2 \psi_l(r_*) + \omega^2 \psi_l(r_*) = V(r) \psi_l(r_*). \quad (45)$$

Here, in this expression r_* is defined as

$$\frac{dr_*}{dr} = \sqrt{g_{rr} |g_{tt}^{-1}|} \quad (46)$$

and is known as the tortoise coordinate. The term $V(r)$ represents the effective potential, whose explicit form is

$$V(r) = |g_{tt}| \left(\frac{l(l+1)}{r^2} + \frac{1}{r\sqrt{|g_{tt}|g_{rr}}} \frac{d}{dr} \sqrt{|g_{tt}|g_{rr}^{-1}} \right), \quad (47)$$

here the term l represents the multipole moment of the black hole's quasinormal modes. In the present work, we will compute the quasinormal modes of the scalar perturbation of the black hole specified by the metric (14) using this potential expression.

B. The asymptotic iteration method

The AIM is an influential mathematical tool employed to solve differential equations numerically, especially to those that are intractable by analytical means. A critical area where AIM is particularly useful to apply is the quasinormal modes of black holes and other systems featuring a potential barrier [163–166]. Quasinormal modes refer to the characteristic oscillations exhibited by a system after a disturbance and are instrumental in analyzing the stability and attributes of black holes. AIM utilizes a systematic iteration approach that facilitates the derivation of precise approximations to the quasinormal modes by converting

the initial differential equation into a series of simpler equations that are readily solvable. The technique has proved successful in various physical systems and remains an active area of exploration.

With the previous definition $u = 1/r$ and following Ref. [163], we obtain the master wave equation for our case as given by

$$\frac{d^2\psi}{du^2} + \frac{\mathcal{Z}'}{\mathcal{Z}} \frac{d\psi}{du} + \left[\frac{\omega^2 - \mathcal{Z} \left(-\frac{2(c_0M + \Lambda)}{u^2} + l(l+1) + 2Mu \right)}{\mathcal{Z}^2} \right] \psi = 0, \quad (48)$$

where the parameter \mathcal{Z} is explicitly given by

$$\mathcal{Z} = -M(c_0 + 2u^3) - \Lambda + u^2. \quad (49)$$

Now, one needs to scale out the divergent characteristics of quasinormal modes at the cosmological horizon, which can be done by defining the wave function $\psi(u)$ as

$$\psi(u) = e^{i\omega r_*} \mathcal{G}(u), \quad (50)$$

which gives us the privilege to have Eq. (48) as

$$\mathcal{Z}\mathcal{G}'' + (\mathcal{Z}' - 2i\omega)\mathcal{G}' - \left[-\frac{2(c_0M + \Lambda)}{u^2} + l(l+1) + 2Mu \right] \mathcal{G} = 0. \quad (51)$$

Again, the correct quasinormal condition at the black hole horizon u_1 results,

$$\mathcal{G}(r_*) = (u - u_1)^{-\frac{i\omega}{\kappa_1}} \chi(r_*), \quad (52)$$

where κ_1 is given by

$$\kappa_1 = \left. \frac{1}{2} \frac{df}{dr} \right|_{r \rightarrow r_1} = Mu_1^2 - \frac{c_0M + \Lambda}{u_1}. \quad (53)$$

In the above expressions, $u_1 = 1/r_1$, where r_1 is the event horizon radius of the black hole. With the new function $\chi(r_*)$, the Eq. (51) takes the conventional format to be used in the iterations of AIM for the differential equation as

$$\chi'' = \lambda_0(u)\chi' + s_0(u)\chi, \quad (54)$$

where the parameters λ_0 and s_0 are defined as

$$\lambda_0(u) = -\frac{1}{\mathcal{Z}} \left[\mathcal{Z}' - \frac{2i\omega}{\kappa_1(u - u_1)} - 2i\omega \right], \quad (55)$$

$$s_0(u) = \frac{1}{\mathcal{Z}} \left[l(l+1) + 2Mu - \frac{2(c_0M + \Lambda)}{u^2} + \frac{i\omega}{\kappa_1(u - u_1)^2} \left(\frac{i\omega}{\kappa_1} + 1 \right) + (\mathcal{Z}' - 2i\omega) \frac{i\omega}{\kappa_1(u - u_1)} \right]. \quad (56)$$

We shall use this differential equation and follow the Ref. [163] to calculate the scalar quasinormal modes for the case of our black hole.

C. The Padé averaged WKB approximation method

Besides the AIM, in this study we use the Padé averaged sixth order WKB approximation method to calculate the quasinormal modes of black hole defined by the metric (14), as mentioned earlier. In this sixth order WKB method, the expression of oscillation frequency ω of GWs can be given by

$$\omega = \sqrt{-i \left[(n + 1/2) + \sum_{k=2}^6 \bar{\Lambda}_k \right] \sqrt{-2V_0''} + V_0}, \quad (57)$$

where $n = 0, 1, 2, \dots$, $V_0 = V(r)|_{r=r_{max}}$ and $V_0'' = \frac{d^2V}{dr^2}|_{r=r_{max}}$. Here r_{max} is the position at which the potential $V(r)$ has its maximum value. $\bar{\Lambda}_k$ are the correction terms and the explicit forms of these correction terms, as well as the Padé averaging recipe, can be found in Ref.s [167–170].

TABLE I: Quasinormal modes from the black hole defined by the metric (14) for different values of the multipole moment l with the overtone number $n = 0$ obtained by using the AIM (with 91 iterations) and the 6th order Padé averaged WKB approximation method. In this calculation we choose the model parameters $c_0 = -0.01$ and $\Lambda = 0.002$. Here we use $M = G = c = \hbar = 1$ unit system.

l	AIM	Padé averaged WKB	Δ_{rms}	Δ_6	Δ_m
1	$0.3271473 - 0.1000942i$	$0.329269 - 0.102651i$	0.00743811	0.000107719	0.97115%
2	$0.5377497 - 0.1048303i$	$0.538571 - 0.104694i$	0.00234137	0.0000262313	0.15196%
3	$0.7481478 - 0.1053878i$	$0.747713 - 0.105344i$	0.000294378	5.808299×10^{-6}	0.05784%
4	$0.9592543 - 0.1056549i$	$0.959321 - 0.105657i$	8.032384×10^{-6}	2.580773×10^{-6}	0.00691%
5	$1.1707337 - 0.1057988i$	$1.171000 - 0.105793i$	0.000233917	1.280549×10^{-6}	0.02266%

In Table I, we list the quasinormal modes for different values of the multipole moment l with overtone number $n = 0$. In the second column, the quasinormal modes obtained from the AIM with 91 iterations are listed and in the third column, the quasinormal modes obtained from the 6th-order Padé averaged WKB approximation method are shown. In this table, Δ_{rms} represents the rms error associated with the Padé averaged 6th order WKB approximation method and Δ_6 provides a measurement of the error from two nearby approximation orders defined as

$$\Delta_6 = \frac{|\omega_7 - \omega_5|}{2}, \quad (58)$$

where ω_5 and ω_7 respectively represent the quasinormal modes calculated by using the Padé averaged 5th order and 7th order WKB approximation methods. In the last column, Δ_m represents the percentage deviation of quasinormal modes calculated by using WKB method from those calculated by using AIM. One can see that with an increase in the multipole moment l , the error associated with the quasinormal modes decreases. It is also seen that the AIM and the Padé averaged 6th-order WKB approximation method provide very close results, that is the quasinormal modes from both methods are in good agreement with each other. Moreover, the agreement between these two methods becomes far better with the increasing l values. It is to be noted that as a characteristic of the WKB approximation method, it fails to provide significant results when the overtone number n is greater than the multipole moment l [85, 87, 90]. Hence, for smaller values of l , it seems that AIM provides more accurate results than those obtained from the WKB method. One may further note that the quasinormal frequencies shown in Table I are in geometric units with $M = 1$. To convert them to physical units, we can use the following conversion formula [171]:

$$f = \frac{32.26}{\eta} (M\omega_R) \text{ kHz}, \quad (59)$$

where $\eta = M/M_\odot$. As mentioned above, in the WKB approximation method, the errors decrease with an increase in $l - n$ and for $n > l$ the method fails to provide actual quasinormal frequencies with a reasonable accuracy [172]. Hence in the rest of the study, we shall consider $n = 0$ and a higher value of l for a better accuracy of the results of quasinormal frequency calculations.

In Fig. 4, we plot the real quasinormal frequencies on the left panel and the imaginary quasinormal frequencies on the right panel with respect to the model parameter c_0 . For both the plots, we use the mass of the black hole $M = 1$, overtone number $n = 0$, and multipole moment $l = 4$. One can see that with an increase in the value of c_0 , the quasinormal frequency decreases non-linearly and approaches zero towards $c_0 = 0.04$. However, beyond $c_0 = 0.04$, oscillation frequencies of quasinormal modes or ringdown GWs start to increase very slowly. So, it seems that the positive values of the model parameter c_0 permit ringdown GWs of very large wavelengths, which will be difficult to detect experimentally. Similarly, the decay rate or the damping rate of the quasinormal modes also decreases non-linearly with an increase in the model parameter c_0 . Near $c_0 = 0.04$, the decay rate also becomes very close to zero. However, beyond this point, the decay rate increases drastically up to $c_0 = 0.1$, representing highly damped GWs.

D. Time domain profiles

In the previous two subsections, we numerically calculated the quasinormal modes and studied their behaviour with respect to the model parameter c_0 . In this subsection, we shall deal with the time domain profiles of the scalar perturbation of the black spacetime. To obtain the time evolution profiles, we shall implement the time domain integration formalism [162]. For this purpose, we define the wavefunction and potential as $\psi(r_*, t) = \psi(i\Delta r_*, j\Delta t) = \psi_{i,j}$ and $V(r(r_*)) = V(r_*, t) = V_{i,j}$. With these definitions we can express radial wave Eq. (45) as

$$\frac{\psi_{i+1,j} - 2\psi_{i,j} + \psi_{i-1,j}}{\Delta r_*^2} - \frac{\psi_{i,j+1} - 2\psi_{i,j} + \psi_{i,j-1}}{\Delta t^2} - V_i \psi_{i,j} = 0. \quad (60)$$

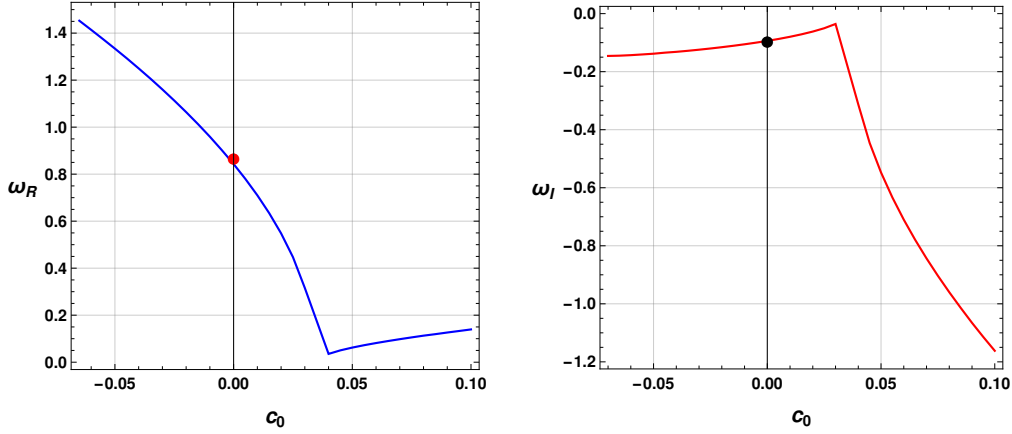


FIG. 4: Variation of real (on the left panel) and imaginary (on the right panel) scalar quasinormal mode frequencies with the model parameter c_0 associated with the black hole metric (14) obtained by using $n = 0, l = 4$ and $\Lambda = 0.002$. Solid circles in both plots denote quasinormal modes for asymptotically flat Schwarzschild black hole. Parameters are expressed in mass units i.e. $M = 1$.

Now, we set the initial conditions $\psi(r_*, t) = \exp\left[-\frac{(r_* - k_1)^2}{2\sigma^2}\right]$ and $\psi(r_*, t)|_{t < 0} = 0$, where k_1 and σ are the median and width of the initial wave-packet, and then calculate the time evolution of the scalar field as

$$\psi_{i,j+1} = -\psi_{i,j-1} + \left(\frac{\Delta t}{\Delta r_*}\right)^2 (\psi_{i+1,j} + \psi_{i-1,j}) + \left(2 - 2\left(\frac{\Delta t}{\Delta r_*}\right)^2 - V_i \Delta t^2\right) \psi_{i,j}. \quad (61)$$

Using the above iteration scheme and choosing a fixed value of $\frac{\Delta t}{\Delta r_*}$, one can easily obtain the profile of ψ with respect to time t . However, one should keep $\frac{\Delta t}{\Delta r_*} < 1$ so that the Von Neumann stability condition is satisfied during the numerical procedure.

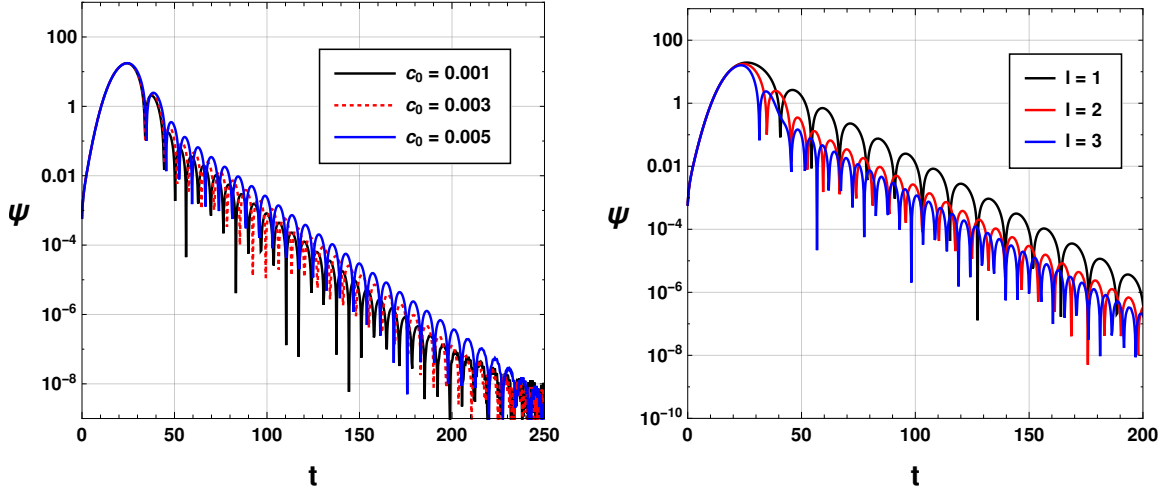


FIG. 5: Time domain profiles with $n = 0$ and $\Lambda = 0.002$ for the massless scalar perturbation. On the left panel, we use $l = 2$ and on the right panel, $c_0 = 0.005$ is used.

Fig. 5 shows the time evolution profiles of the massless scalar field perturbation in the black hole spacetime (14). On the left panel, the time domain profiles are shown for different values of the model parameter c_0 . One can see that with an increase in the value of c_0 from 0.001 to 0.005, the oscillation frequencies decrease slowly. On the right panel, we show the variation of the time domain profiles with different values of the multipole moment l . It is clear from the variation of the time domain profiles that with an increase in the value of the multipole moment l , both the oscillation frequency and the damping rate increase gradually. These results agree well with the numerically calculated quasinormal modes in the previous subsections.

V. OPTICAL BEHAVIOUR OF THE BLACK HOLE

A. Shadow

The shadow of a black hole is the dark area of spacetime that is surrounded by the event horizon of the black hole. Black holes are known to have an intense gravitational pull. The pull is so intense that once it passes the event horizon, even light cannot escape the gravitational attraction [51, 57]. As a result, the area of the black hole creates a shadowy dark zone on the background of the nearby matter or light. The dimension and shape of this shadow can provide vital insights into the characteristics of black holes and the nature of gravity. Recent astronomical and technical developments have made it possible to photograph black hole shadows, significantly advancing our understanding of these mysterious objects [93].

For the case of static and spherically symmetric spacetime metric, the Lagrangian of the form:

$$\mathcal{L}(x, \dot{x}) = \frac{1}{2} g_{\mu\nu} \dot{x}^\mu \dot{x}^\nu, \quad (62)$$

can be written as [116, 117]

$$\mathcal{L}(x, \dot{x}) = \frac{1}{2} \left[-f(r) \dot{t}^2 + \frac{1}{f(r)} \dot{r}^2 + r^2 (\dot{\theta}^2 + \sin^2 \theta \dot{\phi}^2) \right]. \quad (63)$$

Here, the derivative with respect to the proper time τ is indicated by the dot over the variables. The corresponding Euler-Lagrange equation is

$$\frac{d}{d\tau} \left(\frac{\partial \mathcal{L}}{\partial \dot{x}^\mu} \right) - \frac{\partial \mathcal{L}}{\partial x^\mu} = 0. \quad (64)$$

For the present case of the study, choosing the equatorial plane, i.e. $\theta = \pi/2$, the conserved energy \mathcal{E} and angular momentum L can be obtained using killing vectors $\partial/\partial\tau$ and $\partial/\partial\phi$ as [117]

$$\mathcal{E} = f(r) \dot{t}, \quad L = r^2 \dot{\phi}. \quad (65)$$

The geodesic equation for the case of photon results in the relation,

$$-f(r) \dot{t}^2 + \frac{\dot{r}^2}{f(r)} + r^2 \dot{\phi}^2 = 0. \quad (66)$$

In this Eq. (66), using the conserved quantities *i.e.*, \mathcal{E} and L one can obtain the orbital equation of photon as given by [118]

$$\left(\frac{dr}{d\phi} \right)^2 = V_{eff}, \quad (67)$$

where we define the right hand side of Eq. (67) as an effective potential V_{eff} , given by

$$V_{eff} = r^4 \left[\frac{\mathcal{E}^2}{L^2} - \frac{f(r)}{r^2} \right]. \quad (68)$$

Furthermore, by writing Eq. (67) in the form of a radial equation, one can have

$$V_r(r) = \frac{1}{\xi^2} - \dot{r}^2/L^2, \quad (69)$$

where the impact parameter ξ is given as $\xi = L/\mathcal{E}$ and $V_r(r)$ is the reduced potential having the form:

$$V_r(r) = \frac{f(r)}{r^2}. \quad (70)$$

The study of this potential's behaviour with respect to the radial distance r would be the most practical way to comprehend the nature of the photon sphere around the black hole spacetime we have taken into consideration. This potential governs the radial motion of photons in the black hole spacetime. In Fig. 6, we show the behaviour of this potential with respect to r . One can see that the behaviour of the potential is not similar for positive and negative values of the model parameter c_0 . For negative values of the parameter c_0 , it is seen that the potential decreases slowly after reaching a peak point. For smaller values of the parameter

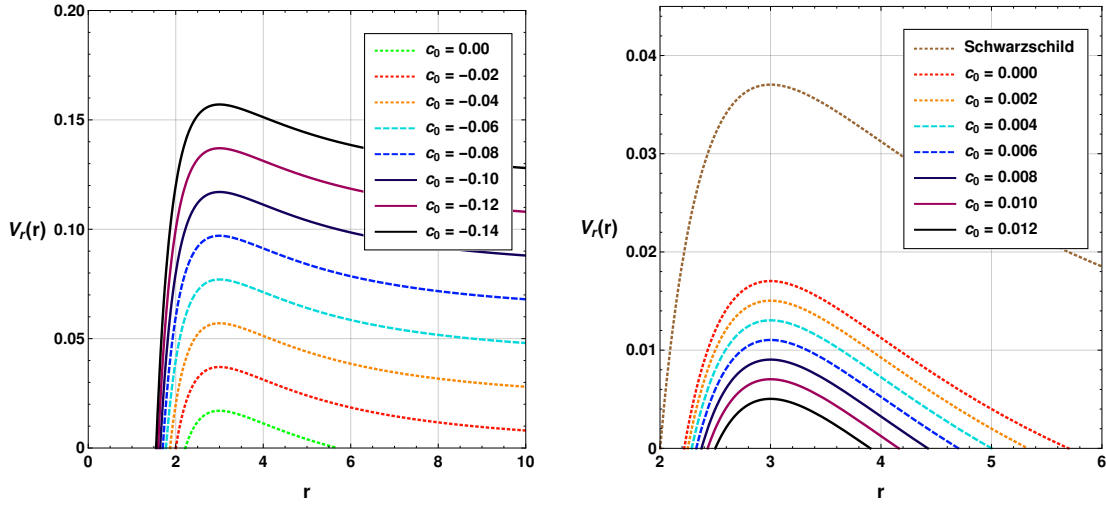


FIG. 6: Variation of the reduced potential $V_r(r)$ with respect to r . In these plots $M = 1$ and $\Lambda = 0.02$ are used.

c_0 , the potential increases to its peak value very swiftly and the peak of the potential increases gradually with a decreasing value of c_0 . On the other hand, for positive values of the parameter c_0 , the peaks are distinct, reach to them comparatively slowly and the potential decreases drastically after reaching the peak with increasing values of r . In this case also, the peak value of the potential increases for lower values of the parameter c_0 . Further, positive c_0 gives a lower peak value and negative c_0 gives a higher peak value than that of the Schwarzschild case.

Considering the turning point of the trajectory, given by $r = r_{ph}$, which is, in fact, the radius of the photon sphere or the light ring surrounding the black hole, one can determine the shadow of the black hole. At this turning point, the following conditions must be satisfied [173–175]:

$$\left. \frac{dr}{d\phi} \right|_{r_{ph}} = 0 \text{ or } V_{eff}|_{r_{ph}} = 0, \text{ and } \left. \frac{d^2r}{d\phi^2} \right|_{r_{ph}} = 0 \text{ or } V'_{eff}|_{r_{ph}} = 0. \quad (71)$$

Using the first condition, the impact parameter ξ at the turning point can be obtained as

$$\frac{1}{\xi_{crit}^2} = \frac{f(r_{ph})}{r_{ph}^2}. \quad (72)$$

The radius of the photon sphere r_{ph} can be determined using the second aforementioned condition and solving the equation:

$$\left. \frac{d}{dr} \mathcal{A}(r) \right|_{r_{ph}} = 0. \quad (73)$$

This equation can be explicitly written as

$$\frac{f'(r_{ph})}{f(r_{ph})} - \frac{h'(r_{ph})}{h(r_{ph})} = 0, \quad (74)$$

where $\mathcal{A}(r) = h(r)/f(r)$ with $h(r) = r^2$. Thus from Eqs. (72) and (74) it is clear that the critical impact parameter is $\xi_{crit} = 3\sqrt{3}M/\sqrt{-27c_0M^3 - 27\Lambda M^2 + 1}$ and the photon sphere is located at $r_{ph} = 3M$.

Now, to obtain the expression for shadow of the black hole, we rewrite Eq. (67) with Eq. (72) in terms of the function $\mathcal{A}(r)$ as

$$\left(\frac{dr}{d\phi} \right)^2 = h(r)f(r) \left(\frac{\mathcal{A}(r)}{\mathcal{A}(r_{ph})} - 1 \right). \quad (75)$$

Using this Eq. (75), the shadow radius can be determined. To this end, if one considers the angle between the light rays from a static observer at r_0 and the radial direction of the photon sphere as α , then this angle can be calculated as [174, 176]

$$\cot \alpha = \frac{1}{\sqrt{f(r)h(r)}} \left. \frac{dr}{d\phi} \right|_{r=r_0}. \quad (76)$$

Together with Eq. (75), above equation can be written as

$$\cot^2 \alpha = \frac{\mathcal{A}(r_0)}{\mathcal{A}(r_{ph})} - 1. \quad (77)$$

Again, above equation can be rewritten using the relation $\sin^2 \alpha = 1/(1 + \cot^2 \alpha)$ as

$$\sin^2 \alpha = \frac{\mathcal{A}(r_{ph})}{\mathcal{A}(r_0)}. \quad (78)$$

Substitution of the actual form of $\mathcal{A}(r_{ph})$ from Eq. (72) and $\mathcal{A}(r_0) = r_0^2/f(r_0)$ the black hole's shadow radius for a static observer at r_0 is estimated as [110]

$$R_s = r_0 \sin \alpha = \sqrt{\frac{r_{ph}^2 f(r_0)}{f(r_{ph})}}. \quad (79)$$

In case of an asymptotically flat black hole and for a static observer at large distance, i.e. at $r_0 \rightarrow \infty$, $f(r_0) \rightarrow 1$. So for such an observer the shadow radius R_s of this type of black hole becomes,

$$R_s = \frac{r_{ph}}{\sqrt{f(r_{ph})}}. \quad (80)$$

The apparent form of the shadow of a black hole can be determined via the stereographic projection of the shadow from the black hole's plane to the observer's image plane with coordinates (X, Y) . These coordinates are defined as [117, 177]

$$X = \lim_{r_0 \rightarrow \infty} \left(-r_0^2 \sin \theta_0 \left. \frac{d\phi}{dr} \right|_{r_0} \right), \quad (81)$$

$$Y = \lim_{r_0 \rightarrow \infty} \left(r_0^2 \left. \frac{d\theta}{dr} \right|_{(r_0, \theta_0)} \right), \quad (82)$$

where θ_0 represents the angular position of the observer with respect to the plane of the black hole. Depending on the value of c_0 , the black hole spacetime can be de-Sitter (dS) or Anti de-Sitter (AdS) for a fixed value of Λ . It is to be noted that dS solution gives rise to two horizons viz., event horizon and cosmological horizon, whereas AdS has only event horizon similar to the case of the Schwarzschild black hole. In general, one may note that physical observers can be present between the event horizon and cosmological horizon with different physically allowed observer distance i.e. $r_1 < r_0 < r_\Lambda$, where r_1 and r_Λ are the event and cosmological horizons respectively. Hence a variation in r_0 can have impacts on the appearance of the black hole shadow [176]. On the other hand, for the asymptotically flat black holes with a static observer at large distance scenario as mentioned above, the apparent form of the shadow remains independent of the observer position. Therefore, in this investigation, we use the shadow radius expression (79) to obtain the stereographic projections of the black hole shadow at some finite physical observer distance r_0 .

For the black hole considered in this study, the stereographic projections of the black hole shadow at finite observer distances are shown in Fig. 7. On the left panel, we show the behaviour of the black hole shadow radius for different values of the black hole mass M . In this case, we observe that the shadow radius increases with an increase in the value of black hole mass M at finite observer distance $r_0 = 10$. On the right panel, we show the dependency of the black hole shadow with the model parameter c_0 . With an increase in the value of the parameter c_0 , we observe a decrease in the size of the black hole shadow at finite observer distance $r_0 = 15$. That is, the size of the black hole shadow is bigger for the AdS ones than that of the dS cases. Finally, in Fig. 8, we show the dependency of the shadow radius with the observer distance r_0 for both dS and AdS black holes considering $\Lambda = 0.002$ and $M = 1$. For the dS case (left panel) we choose the model parameter $c_0 = 0.001$ for which the black hole can have two horizons at $r = 2.02491$ (event horizon) and $r = 17.1606$ (cosmological horizon). The physical observer distance should lie within this range. We consider $r_0 = 10$ to 16 to obtain the stereographic projections of the black hole shadow. For comparison, we have also plotted the Schwarzschild black hole shadow at infinite observer distance. It is clear from the figure that the observer distance plays a crucial role in depicting the black hole shadow radius. In this dS case, we see that with an increase in the observer distance r_0 , the shadow radius decreases and they are smaller than the Schwarzschild black hole shadow. In the case of AdS black holes we take the parameter $c_0 = -0.003$ (right panel). It is seen that with an increase in the distance r_0 of the observer the shadow size increases and is comparable to that of the Schwarzschild black one, in contrast to the case of dS black holes.

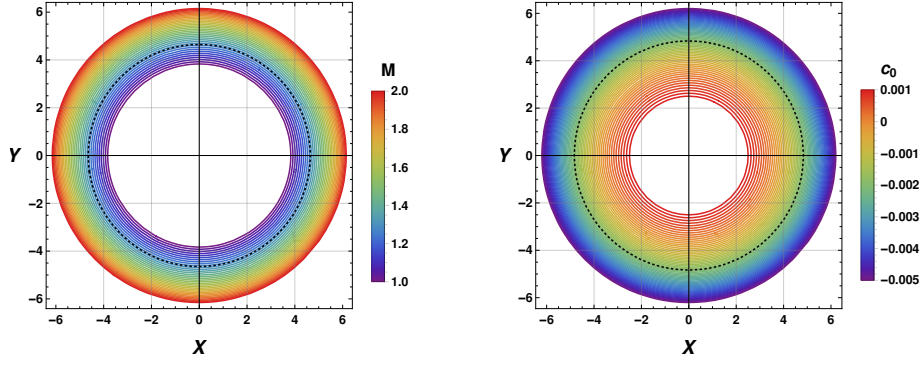


FIG. 7: Stereographic projections of the shadow of the black hole with $\Lambda = 0.002$. On the left panel, we use $c_0 = 0.001$ and $r_0 = 10$ and on the right panel, $M = 1$ and $r_0 = 15$. The black dotted circle in both cases denote Schwarzschild black hole shadow radius at respective finite observer distances.

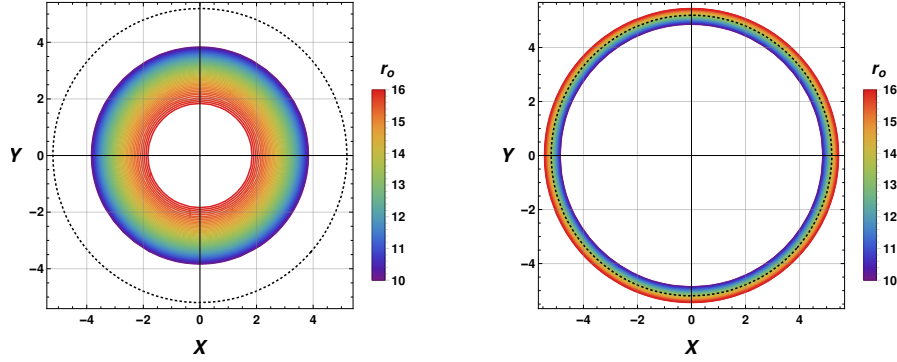


FIG. 8: Stereographic projections of the shadow of the black hole with $\Lambda = 0.002$ and $M = 1$. On the left panel, we use $c_0 = 0.001$ (dS case) and on the right panel, $c_0 = -0.003$ (AdS case). The black dotted circle in each plot denotes the Schwarzschild black hole shadow radius at infinite observer distance (i.e. at $r_0 \rightarrow \infty$).

B. Emission rate

By examining the black hole shadow, it is possible to investigate the emission of particles in the vicinity of the black hole. It has been demonstrated that for an observer located far away, the black hole shadow is indicative of its high-energy absorption cross-section [138]. Generally speaking, in the case of a spherically symmetric black hole, the absorption cross-section exhibits oscillatory behaviour around a constant limiting value σ_{lim} at extremely high energies. This limiting value σ_{lim} corresponds to the geometrical cross-section of the photon sphere around the black hole. Since the shadow provides a means of visually detecting a black hole, it is roughly equivalent to the area of the photon sphere ($\sigma_{lim} \approx \pi R_s^2$). Thus the energy emission rate can be calculated by using the equation [138],

$$\frac{d^2 E(\omega_p)}{dt d\omega_p} = \frac{2\pi^3 \omega_p^3 R_s^2}{e^{\omega_p/T} - 1}, \quad (83)$$

in which ω_p is the emission frequency, and T is Hawking temperature given by

$$T = \frac{\hbar f'(r_h)}{4\pi}, \quad (84)$$

where r_h is the horizon radius of the black hole.

Using the expression of Hawking temperature (84) in Eq. (83), we show the variation of the emission rate with respect to ω_p for different values of c_0 in Fig. 9. One can see that with an increase in the value of the parameter c_0 , the emission rate of the black hole decreases. Hence for smaller values of the parameter c_0 , the black hole will evaporate more rapidly. Moreover, it is to be noted that for $c_0 < -0.01$ the emission rate is greater than that of the Schwarzschild black hole, whereas it is less than

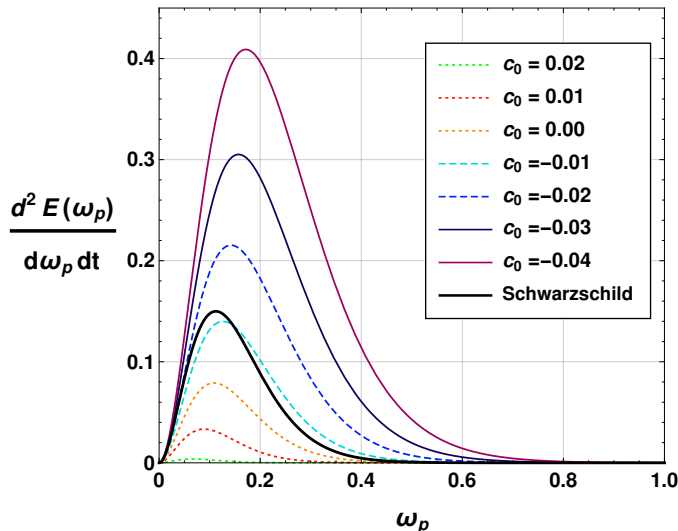


FIG. 9: Emission rate of the black hole with respect to emission frequency ω_p for $M = 1$, $\Lambda = 0.002$ and observer distance $r_0 = 5$.

Schwarzschild one for the positive values of c_0 . For the $c_0 = -0.01$ case, the rate is very close to the Schwarzschild black hole. Here we consider the observer distance $r_0 = 5$, the cosmological constant $\Lambda = 0.002$ and the black hole mass $M = 1$. Thus in this figure the cases for $c_0 \leq -0.01$ correspond to the AdS black holes situations, whereas other values of c_0 correspond to the dS black holes.

VI. CONCLUSION

In this work, we study a recently introduced static black hole solution in an extension of modified teleparallel gravity i.e., $f(\mathcal{T}, \mathcal{B})$ modified gravity, which includes the function of the torsion scalar \mathcal{T} and a related boundary term \mathcal{B} . In this modified gravity theory, we compute the deflection angle of light by a non-asymptotically flat black hole. Then we study the quasinormal modes associated with the axial scalar perturbation in the background of the black hole.

Gibbons and Werner first introduced an alternative way to calculate the gravitational bending angle using the Gauss-Bonnet theorem. They first evaluated the deflection angle for a Schwarzschild black hole. Since then their work has been extended in various ways for different kinds of black holes. Few researchers have computed the deflection angle from the stationary black holes. Few have again considered finite distances between source and receiver, and derived the deflection angle by the static as well as stationary black holes. Some recent studies also considered black holes in modified gravity theories to obtain the deflection angle of light. In this work, we implemented the Ishihara *et al.* method to evaluate the deflection angle of light from the receiver point of view. This method does not depend on the asymptotic flatness. Hence, we have applied this method in the non-asymptotically flat black hole in $f(\mathcal{T}, \mathcal{B})$ gravity. We have computed the bending angle considering the source and the receiver at a finite distance. It is found that when the source and the receiver are considered near to the lens object, the deflection angle becomes divergent. The boundary term coming from $f(\mathcal{T}, \mathcal{B})$ gravity has a significant effect on the deflection angle. In the near future, we wish to extend our work to obtain the deflection angle of massive particles using Ishihara *et al.* method in the black hole as well as in wormhole backgrounds in different MTGs.

Quasinormal modes are some complex numbers related to the emission of GWs from the compact objects in the universe. The real part of these modes is related to the emission frequency and the imaginary part is related to the damping. In this work, we try to find a Schrödinger type equation containing an effective potential, which allows us to compute the quasinormal modes associated with the massless scalar perturbations in the background of the considered black hole in the $f(\mathcal{T}, \mathcal{B})$ gravity. For this purpose, we use the AIM and Padé averaged sixth-order WKB approximation method. We obtained the quasinormal modes for different values of the multipole moment l with the overtone number $n = 0$. It has been observed that for smaller values of l , the error associated with the quasinormal frequencies calculated with WKB method is higher in magnitude. With an increase in the value of l , the errors associated with the frequencies decrease significantly. The AIM stands in agreement with the results obtained by using the WKB method, confirming the validity of the results. Our study shows that the parameter c_0 has a significant impact on the quasinormal modes of the black hole. Moreover, the time domain profile analysis of evolution of massless scalar field perturbation in the black hole spacetime also confirms all these outcomes of quasinormal modes' calculations. However, for the observational constraints on the model from the quasinormal modes, we might need to wait for the LISA [87]. The reason

behind this is that assuming the nearest black holes, such as Sgr A* or M 87* to be almost static, their respective quasinormal modes are beyond the sensitivity range of current and near future ground-based detectors [87]. Nonetheless, the upcoming LISA space-based detector exhibits a remarkable increase in sensitivity and will be proficient in detecting quasinormal modes with a greater precision.

We also study the optical properties of the black hole *viz.*, the shadow and the emission rate. It is seen from our investigation that the shadow of the black hole decreases with an increase in the value of the parameter c_0 . Similarly, an increase in the value of c_0 decreases the emission rate or evaporation rate of the black hole, hence increasing its stability.

Our investigation demonstrates that the boundary-derived parameter c_0 exerts considerable influence on the spacetime of a black hole, impacting various observable characteristics of it. We demonstrate that c_0 has effects on the gravitational deflection of light, ringdown GWs or quasinormal modes, the black hole shadow and the emission rate, potentially providing observable evidence for $f(\mathcal{T}, \mathcal{B})$ gravity. Constraining the model with available observational data will provide more useful insights into the $f(\mathcal{T}, \mathcal{B})$ gravity which we keep as a future prospect of our study.

Acknowledgments

UDG is thankful to the Inter-University Centre for Astronomy and Astrophysics (IUCAA), Pune, India for the Visiting Associateship of the institute.

-
- [1] A. Einstein, *The Foundation of the General Theory of Relativity*, *Ann. Phys. (N.Y.)* **49**, 769 (1916), **14**, 517 (2005).
- [2] A. G. Reiss et al., *Observational Evidence from Supernovae for an Accelerating Universe and a Cosmological Constant*, *Astron. J.* **116**, 1009 (1998).
- [3] S. Perlmutter et al., *Measurements of Ω and Λ from 42 High-Redshift Supernovae*, *Astrophys. J.* **517**, 565 (1999).
- [4] V. C. Rubin, N. Thonnard and W. K. Ford Jr., *Rotational properties of 21 SC galaxies with a large range of luminosities and radii, from NGC 4605 ($R = 4$ kpc) to UGC 2885 ($R = 122$ kpc)*, *Astrophys. J.* **238**, 471-487 (1980).
- [5] Bing-Lin Young, *A survey of dark matter and related topics in cosmology*, *Front. Phys.* **12**, 121201 (2017).
- [6] T. Harko, *Galactic rotation curves in modified gravity with nonminimal coupling between matter and geometry*, *Phys. Rev. D* **81**, 084050 (2010).
- [7] L. Á. Gergely et al., *Galactic rotation curves in brane world models*, *Mon. Not. R. Astron. Soc.* **415**, 3275-3290 (2011).
- [8] N. Parbin and U. D. Goswami, *Galactic rotation dynamics in a new $f(\mathcal{R})$ gravity model*, [arXiv:2208.06564].
- [9] G. Bertone and D. Hooper, *History of Dark Matter*, *Rev. Mod. Phys.* **90**, 045002 (2018).
- [10] J. G. de Swart, G. Bertone and J. van Dongen, *How Dark Matter Came to Matter*, *Nature Astron.* **1**, 0059 (2017).
- [11] G. Bertone and T. M. P. Tait, *A New Era in the Search for Dark Matter*, *Nature* **562**, 51-56 (2018).
- [12] C. S. Frenk and S. D. M. White, *Dark Matter and Cosmic Structure*, *Ann. Phys. (Berlin)*, 507534 (2012).
- [13] L. E. Strigari, *Galactic Searches for Dark Matter*, *Phys. Rep.* **531**, 1-88 (2013).
- [14] C. M. Will, *The Confrontation between General Relativity and Experiment*, *Living Rev. Relativ.* **17**, 4 (2014).
- [15] T. Clifton, *Alternative Theories of Gravity*, [arXiv:gr-qc/0610071] (2006).
- [16] R. V. Wagoner, *Scalar-Tensor Theory and Gravitational Waves*, *Phys. Rev. D* **1**, 3209 (1970).
- [17] R. W. Hellings and K. Nordtvedt, Jr., *Vector-Metric Theory of Gravity*, *Phys. Rev. D* **7**, 3593 (1973).
- [18] S. Capozziello and M. De Laurentis, *Extended Theories of Gravity*, *Phys. Rep.* **509**, 167-321 (2011).
- [19] T. Clifton et al., *Modified Gravity and Cosmology*, *Phys. Rep.* **513**, 1-189 (2012).
- [20] S. Nojiri, S.D. Odintsov and V.K. Oikonomou, *Modified Gravity Theories on a Nutshell: Inflation, Bounce and Late-Time Evolution*, *Phys. Rept.* **692**, 1-104 (2017).
- [21] S. Nojiri and S.D. Odintsov, *Unified Cosmic History in Modified Gravity: From $F(R)$ Theory to Lorentz Non-Invariant Models*, *Phys. Rept.* **505**, 59-144 (2011).
- [22] S. Nojiri and S.D. Odintsov, *Dark Energy, Inflation and Dark Matter from Modified $F(R)$ Gravity*, *TSPU Bulletin N* **8(110)**, 7 (2011) [arXiv:0807.0685].
- [23] D. J. Gogoi and U. D. Goswami, *A New $f(R)$ Gravity Model and Properties of Gravitational Waves in It*, *Eur. Phys. J. C* **80**, 1101 (2020).
- [24] N. Parbin and U. D. Goswami, *Scalarons Mimicking Dark Matter in the Hu-Sawicki Model of $f(R)$ Gravity*, *Mod. Phys. Lett. A* **36**, 2150265 (2021).
- [25] J. Bora, D. J. Gogoi and U. D. Goswami, *Strange stars in $f(R)$ gravity Palatini formalism and gravitational wave echoes from them*, *JCAP* **09**, 057 (2022).
- [26] D. J. Gogoi and U. D. Goswami, *Cosmology with a new $f(R)$ gravity model in Palatini formalism*, *Int. J. Mod. Phys. D* **31**, 2250048 (2022).
- [27] F. W. Dyson et al., *IX. A Determination of the Deflection of Light by the Sun's Gravitational Field, from Observations Made at the Total Eclipse of May 29, 1919*, *Phil. Trans. R. Soc. A* **220**, 291 (1920).
- [28] P. Schneider et al., *Gravitational lenses* (Berlin: Springer) (<https://doi.org/10.1007/978-3-662-03758-4>) (1992).
- [29] V. Trimble, *The first lenses Gravitational Lensing: Recent Progress and Future Goals* (ASP Conference Series vol 237) ed T G Brainerd and C S Kochanek (San Francisco, CA: Astronomical Society of the Pacific) pp 1-13 (2001).

- [30] J. Renn et al., *The Origin of Gravitational Lensing: A Postscript to Einstein's 1936 Science Paper*, *Science* **275**, 184-6 (1997).
- [31] D. Valls-Gabaud, *The Conceptual Origins of Gravitational Lensing*, *AIP Conf. Proc.* **861**, 1163-71 (2006).
- [32] P. Young et al., *The Double Quasar Q0957+561 A, B: A Gravitational Lens Image Formed by a Galaxy at $Z=0.39$* , *Astrophys. J.* **241**, 507-520 (1980).
- [33] K. S. Virbhadra and G. F. R. Ellis, *Schwarzschild black hole lensing*, *Phys. Rev. D* **62**, 084003 (2000).
- [34] F. Zhao et al., *Gravitational lensing effects of a Reissner–Nordström–de Sitter black hole*, *Phys. Rev. D* **93**, 123017 (2016).
- [35] W. Rindler and M. Ishak, *Contribution of the cosmological constant to the relativistic bending of light revisited*, *Phys. Rev. D* **76**, 043006 (2007).
- [36] K. S. Virbhadra and G. F. R. Ellis, *Gravitational lensing by naked singularities*, *Phys. Rev. D* **65**, 103004 (2002).
- [37] R. Shaikh et al., *Analytical approach to strong gravitational lensing from ultracompact objects*, *Phys. Rev. D* **99**, 104040 (2019).
- [38] M. P. Do Carmo, *Differential geometry of curves and surfaces* (Dover Publications, Mineola, New York) (2016).
- [39] W. Klingenberg, *A Course in Differential Geometry* (Springer-Verlag, New York) (1978).
- [40] G. W. Gibbons and M. C. Werner, *Applications of the Gauss-Bonnet theorem to gravitational lensing*, *Class. Quantum Grav.* **25**, 235009 (2008).
- [41] K. Jusufi et al., *Light deflection by a rotating global monopole spacetime*, *Phys. Rev. D* **95**, 104012 (2017).
- [42] K. Jusufi, *Gravitational lensing by Reissner–Nordström black holes with topological defects*, *Astrophys. Space Sci.* **361**, 24 (2016).
- [43] K. Jusufi, *Light Deflection with Torsion Effects Caused by a Spinning Cosmic String*, *Eur. Phys. J. C* **76**, 332 (2016).
- [44] K. Jusufi, I. Sakalli and A. Övgün, *Effect of Lorentz Symmetry Breaking on the Deflection of Light in a Cosmic String Spacetime*, *Phys. Rev. D* **96**, 024040 (2017).
- [45] K. Jusufi, *Quantum Effects on the Deflection of Light and the Gauss-Bonnet Theorem*, *Int. J. Geom. Methods Mod. Phys.* **14**, 1750137 (2017).
- [46] I. Sakalli and A. Övgün, *Hawking Radiation and Deflection of Light from Rindler Modified Schwarzschild Black Hole*, *EPL* **118**, 60006 (2017).
- [47] A. Övgün, G. Gulchev and K. Jusufi, *Weak Gravitational Lensing by Phantom Black Holes and Phantom Wormholes Using the Gauss-Bonnet Theorem*, *Ann. of Phys.* **406**, 152-172 (2019).
- [48] A. Övgün, *Weak Field Deflection Angle by Regular Black Holes with Cosmic Strings Using the Gauss-Bonnet Theorem*, *Phys. Rev. D* **99**, 104075 (2019).
- [49] Z. Li and A. Övgün, *Finite-Distance Gravitational Deflection of Massive Particles by a Kerr-like Black Hole in the Bumblebee Gravity Model*, *Phys. Rev. D* **101**, 024040 (2020).
- [50] S. K. Jha and A. Rahaman, *Gravitational Lensing by the Hairy Schwarzschild Black Hole* [arXiv:2205.06052].
- [51] B. Eslam Panah, Kh. Jafarzade and S. H. Hendi, *Charged 4D Einstein-Gauss-Bonnet-AdS Black Holes: Shadow, Energy Emission, Deflection Angle and Heat Engine*, *Nuclear Physics B* **961**, 115269 (2020).
- [52] B. E. Panah, Kh. Jafarzade and A. Rincon, *Three-Dimensional AdS Black Holes in Massive-Power-Maxwell Theory* [arXiv:2201.13211].
- [53] M. C. Werner, *Gravitational Lensing in the Kerr-Randers Optical Geometry*, *Gen. Relativ. Gravit.* **44**, 3047-3057 (2012).
- [54] K. Jusufi et al., *Deflection of Light by Rotating Regular Black Holes Using the Gauss-Bonnet Theorem*, *Phys. Rev. D* **97**, 124024 (2018).
- [55] A. Ishihara et al., *Gravitational Bending Angle of Light for Finite Distance and the Gauss-Bonnet Theorem*, *Phys. Rev. D* **94**, 084015 (2016).
- [56] T. Ono, A. Ishihara and H. Asada, *Gravitomagnetic Bending Angle of Light with Finite-Distance Corrections in Stationary Axisymmetric Spacetimes*, *Phys. Rev. D* **96**, 104037 (2017).
- [57] R. Kumar, S. G. Ghosh and A. Wang, *Shadow Cast and Deflection of Light by Charged Rotating Regular Black Hole*, *Phys. Rev. D* **100**, 124024 (2019).
- [58] R. Kumar, S. G. Ghosh and A. Wang, *Gravitational Deflection of Light and Shadow Cast by Rotating Kalb-Ramond Black Holes*, *Phys. Rev. D* **101**, 104001 (2020).
- [59] T. Zhu et al., *Shadows and Deflection Angle of Charged and Slowly Rotating Black Holes in Einstein-Æther Theory*, *Phys. Rev. D* **100**, 044055 (2019).
- [60] G. Crisnejo, E. Gallo and K. Jusufi, *Higher Order Corrections to Deflection Angle of Massive Particles and Light Rays in Plasma Media for Stationary Spacetimes Using the Gauss-Bonnet Theorem*, *Phys. Rev. D* **100**, 104045 (2019).
- [61] T. Ono and H. Asada, *The Effects of Finite Distance on the Gravitational Deflection Angle of Light*, *Universe* **5**, 218 (2019).
- [62] K. Takizawa, T. Ono and H. Asada, *Gravitational Deflection Angle of Light: Definition by an Observer and Its Application to an Asymptotically Nonflat Spacetime*, *Phys. Rev. D* **101**, 104032 (2020).
- [63] I. D. D. Carvalho et al., *The Gravitational Bending Angle by Static and Spherically Symmetric Black Holes in Bumblebee Gravity* [arXiv:2103.03845].
- [64] K. Jusufi et al., *Testing Born–Infeld $f(T)$ Teleparallel Gravity through Sgr A* Observations*, *Eur. Phys. J. C* **82**, 1018 (2022).
- [65] R. C. Pantig and A. Övgün, *Dark Matter Effect on the Weak Deflection Angle by Black Holes at the Center of Milky Way and M87 Galaxies* *Eur. Phys. J. C* **82**, 391 (2022).
- [66] R. C. Pantig et al., *Shadow and Weak Deflection Angle of Extended Uncertainty Principle Black Hole Surrounded with Dark Matter*, *Ann. of Phys.* **436**, 168722 (2022).
- [67] W. Javed et al., *Weak Deflection Angle by Kalb-Ramond Traversable Wormhole in Plasma and Dark Matter Mediums*, *Preprints* (2022).
- [68] A. Övgün, *Weak Deflection Angle of Black-Bounce Traversable Wormholes Using Gauss–Bonnet Theorem in the Dark Matter Medium*, *Turk. J. Phys.* **44**, 465-471 (2020).
- [69] S. Bahamonde, C.G. Böhmer and M. Wright, *Modified teleparallel theories of gravity*, *Phys. Rev. D* **92**, 104042 (2015). [arXiv:1508.05120]
- [70] S. Bahamonde and S. Capozziello, *Noether Symmetry Approach in $f(T,B)$ Teleparallel Cosmology*, *Eur. Phys. J. C* **77**, 107 (2017).
- [71] S. Bahamonde, M. Zubair and G. Abbas, *Thermodynamics and Cosmological Reconstruction in $f(T,B)$ Gravity*, *Physics of the Dark*

- Universe **19**, 78 (2018).
- [72] S. Capozziello, M. Capriolo and L. Caso, *Weak Field Limit and Gravitational Waves in $f(T,B)$ Teleparallel Gravity*, *Eur. Phys. J. C* **80**, 156 (2020).
- [73] G. Farrugia, J. L. Said and A. Finch, *Gravitoelectromagnetism, Solar System Tests, and Weak-Field Solutions in $f(T,B)$ Gravity with Observational Constraints*, *Universe* **6**, 34 (2020).
- [74] S. Bahamonde et al., *Black Holes in $f(T,B)$ Gravity: Exact and Perturbed Solutions*, *J. Cosmol. Astropart. Phys.* **2022**, 037 (2022).
- [75] S. Bahamonde et al., *Scalar-Tensor Teleparallel Wormholes by Noether Symmetries*, *Phys. Rev. D* **94**, 084042 (2016).
- [76] J. Rayimbaev et al., *Quasiperiodic Oscillations, Quasinormal Modes and Shadows of Bardeen-Kiselev Black Holes*, *Phys. Dark Univ.* **35**, 100930 (2022).
- [77] M. Ghasemi-Nodehi et al., *Shadow, Quasinormal Modes, and Quasiperiodic Oscillations of Rotating Kaluza-Klein Black Holes*, *Phys. Rev. D* **102**, 104032 (2020).
- [78] C.V. Vishveshwara, *Stability of the Schwarzschild metric*, *Phys. Rev. D* **1** 2870 (1970).
- [79] W.H. Press, *Long Wave Trains of Gravitational Waves from a Vibrating Black Hole*, *Astrophys. J. Lett.* **170** L105 (1971).
- [80] S. Chandrasekhar and S.L. Detweiler, *The quasi-normal modes of the Schwarzschild black hole*, *Proc. Roy. Soc. Lond. A* **344** 441 (1975).
- [81] S. Chandrasekhar, *The mathematical theory of black holes*, Oxford University Press, Oxford (1992).
- [82] C. Ma et al., *Massive scalar field quasinormal modes of a Schwarzschild black hole surrounded by quintessence*, *Central Eur. J. Phys.* **6**, 194 (2008).
- [83] D. Liang et al., *Polarizations of gravitational waves in $f(R)$ gravity*, *Phys. Rev. D* **95**, 104034 (2017).
- [84] R. Oliveira, D.M. Dantas and C.A.S. Almeida, *Quasinormal frequencies for a black hole in a bumblebee gravity*, *EPL* **135**, 10003 (2021).
- [85] D. J. Gogoi and U. D. Goswami, *Quasinormal modes of black holes with non-linear-electrodynamic sources in Rastall gravity*, *Phys. Dark Univ.* **33**, 100860 (2021).
- [86] J.P. Morais Graça and I.P. Lobo, *Scalar QNMs for higher dimensional black holes surrounded by quintessence in Rastall gravity*, *Eur. Phys. J. C* **78**, 101 (2018).
- [87] D. J. Gogoi and U. D. Goswami, *Quasinormal Modes and Hawking Radiation Sparsity of GUP Corrected Black Holes in Bumblebee Gravity with Topological Defects*, *JCAP* **06**, 029 (2022).
- [88] D. J. Gogoi and U. D. Goswami, *Gravitational Waves in $f(R)$ Gravity Power Law Model*, *Indian J. of Phys.* **96**, 637 (2022).
- [89] D. J. Gogoi, R. Karmakar, and U. D. Goswami, *Quasinormal Modes of Non-Linearly Charged Black Holes Surrounded by a Cloud of Strings in Rastall Gravity*, *Int. J. Geom. Methods Mod. Phys.* **20**, 2350007 (2023).
- [90] D. J. Gogoi and U. D. Goswami, *Tideless Traversable Wormholes surrounded by cloud of strings in $f(R)$ gravity*, *JCAP* **02**, 027 (2023).
- [91] R. Karmakar, D. J. Gogoi and U. D. Goswami, *Quasinormal modes and thermodynamic properties of GUP-corrected Schwarzschild black hole surrounded by quintessence*, *Int. J. Mod. Phys. A* **37**, 2250180 (2022).
- [92] A. Övgün, I. Sakalli and J. Saavedra, *Shadow Cast and Deflection Angle of Kerr-Newman-Kasuya Spacetime*, *J. Cosmol. Astropart. Phys.* **10**, 041 (2018).
- [93] S.-W. Wei and Y.-X. Liu, *Observing the Shadow of Einstein-Maxwell-Dilaton-Axion Black Hole*, *J. Cosmol. Astropart. Phys.* **11**, 063 (2013).
- [94] P. V. P. Cunha et al., *Shadows of Einstein–Dilaton–Gauss–Bonnet Black Holes*, *Physics Letters B* **768**, 373 (2017).
- [95] H.-M. Wang, Y.-M. Xu and S.-W. Wei, *Shadows of Kerr-like Black Holes in a Modified Gravity Theory*, *J. Cosmol. Astropart. Phys.* **03**, 046 (2019).
- [96] S. Dastan, R. Saffari and S. Soroushfar, *Shadow of a Charged Rotating Black Hole in $f(R)$ Gravity*, *Eur. Phys. J. Plus* **137**, 1002 (2022).
- [97] Z. Li and C. Bambi, *Measuring the Kerr spin parameter of regular black holes from their shadow*, *JCAP* **1401**, 041 (2014).
- [98] G. Gylchev, P. Nedkova, V. Tinchev and S. Yazadjiev, *On the shadow of rotating traversable wormholes*, *Eur. Phys. J. C* **78** (7), 544 (2018).
- [99] C. Bambi and K. Freese, *Apparent shape of super-spinning black holes*, *Phys. Rev. D* **79**, 043002 (2009).
- [100] S. Haroon, K. Jusufi and M. Jamil, *Shadow Images of a Rotating Dyonic Black Hole with a Global Monopole Surrounded by Perfect Fluid*, *Universe* **6** (2), 23 (2020).
- [101] M. Okyay and A. Övgün, *Nonlinear electrodynamics effects on the black hole shadow, deflection angle, quasinormal modes and greybody factors*, *JCAP* **01**, 009 (2022).
- [102] A. Belhaj and Y. Sekhmani, *Shadows of rotating quintessential black holes in Einstein–Gauss–Bonnet gravity with a cloud of strings*, *Gen. Relativ Gravit.* **54** (2021).
- [103] A. Allahyari, M. Khodadi, S. Vagnozzi and D. F. Mota, *Magnetically charged black holes from non-linear electrodynamics and the Event Horizon Telescope*, *JCAP* **02**, 003 (2020).
- [104] C. Bambi, K. Freese, S. Vagnozzi and L. Visinelli, *Testing the rotational nature of supermassive object M87* from the circularity and size of its first image*, *Phys. Rev. D* **100**, 044057 (2019).
- [105] S. Vagnozzi, C. Bambi and L. Visinelli, *Concerns regarding the use of black hole shadows as standard rulers*, *Class. Quantum Grav.* **37**, 087001 (2020).
- [106] M. Khodadi, A. Allahyari, S. Vagnozzi and D. F. Mota, *Black holes with scalar hair in light of the Event Horizon Telescope*, *JCAP* **09**, 026 (2020).
- [107] R. Roy, S. Vagnozzi and L. Visinelli, *Superradiance evolution of black hole shadows revisited*, *Phys. Rev. D* **105**, 083002 (2022).
- [108] B. E. Panah, Kh. Jafarzade and A. Rincon, *Three-dimensional AdS black holes in massive-power-Maxwell theory*, [arXiv:2201.13211v1] (2022).
- [109] R. Ghosh, M. Rahman and A. K. Mishra, *Regularized Stable Kerr Black Hole: Cosmic Censorships, Shadow and Quasi-Normal Modes*, arXiv:2209.12291 [gr-qc] (2023).

- [110] R. A. Konoplya, *Shadow of a black hole surrounded by dark matter*, *Phys. Lett B* **795**, 1-6 (2019).
- [111] R. A. Konoplya and A. Zhidenko, *Shadows of parametrized axially symmetric black holes allowing for separation of variables*, *Phys. Rev. D* **103**, 104033 (2021).
- [112] K. Jusufi and Saurabh, *Black hole shadows in Verlinde's emergent gravity*, *MNRAS* **503**, 1310 (2021).
- [113] T. Zhu, Q. Wu, M. Jamil and K. Jusufi, *Shadows and deflection angle of charged and slowly rotating black holes in Einstein-Æther theory*, *Phys. Rev. D* **100**, 044055 (2019).
- [114] K. Jusufi et al., *Black hole surrounded by a dark matter halo in the M87 galactic center and its identification with shadow images*, *Phys. Rev. D* **100**, 044012 (2019).
- [115] K. Jusufi, *Quasinormal Modes of Black Holes Surrounded by Dark Matter and Their Connection with the Shadow Radius*, *Phys. Rev. D* **101**, 084055 (2020).
- [116] R. C. Pantig, L. Mastrototaro, G. Lambiase, and A. Övgün, *Shadow, Lensing, Quasinormal Modes, Greybody Bounds and Neutrino Propagation by Dyonic ModMax Black Holes*, *Eur. Phys. J. C* **82**, 1155 (2022).
- [117] R. Karmakar, D. J. Gogoi and U. D. Goswami, *Thermodynamics and Shadows of GUP-corrected Black Holes with Topological Defects in Bumblebee Gravity*, arXiv:2303.00297 (2023).
- [118] İ. Çimdiker, D. Demir, and A. Övgün, *Black Hole Shadow in Symmergent Gravity*, *Physics of the Dark Universe* **34**, 100900 (2021).
- [119] B. McInnes and Y. C. Ong, *Event horizon wrinklification*, *Class. quantum Grav.* **38**, 034002 (2021).
- [120] M. Khodadi, E. N. Saridakis, *Einstein-Æther gravity in the light of event horizon telescope observations of M87**, *Physics of the Dark Universe* **32**, 100835 (2021).
- [121] K. Glampedakis and G. Pappas, *Can supermassive black hole shadows test the Kerr metric?*, *Phys. Rev. D* **104**, L081503 (2021).
- [122] S. Devi, A. Nagarajan S., S. Chakrabarty and B. R. Majhi, *Shadow of quantum extended Kruskal black hole and its super-radiance property*, *Physics of the Dark Universe* **39**, 101173 (2023).
- [123] M. Khodadi, G. Lambiase and D. Mota, *No-hair theorem in the wake of Event Horizon Telescope*, *JCAP* **09** 028 (2021).
- [124] M. Khodadi and G. Lambiase, *Probing Lorentz symmetry violation using the first image of Sagittarius A*: Constraints on standard-model extension coefficients*, *Phys. Rev. D* **106**, 104050 (2022).
- [125] I. Banerjee, S. Chakrabarty and S. SenGupta, *Hunting extra dimensions in the shadow of Sgr A**, *Phys. Rev. D* **106**, 084051 (2022).
- [126] M. Afrin, S. Vagnozzi and S. G. Ghosh, *Tests of Loop Quantum Gravity from the Event Horizon Telescope Results of Sgr A**, *APJ* **944**, 2 (2023).
- [127] M. Khodadi, *Shadow of black hole surrounded by magnetized plasma: Axion-plasmon cloud*, *Nuclear Phys. B* **985**, 116014 (2022).
- [128] S. Chen, J. Jing, W. L. Qian and B. Wang, *Black hole images: A Review*, *Sci. China Phys. Mech. Astron.* **66**, 260401 (2023).
- [129] S. Vagnozzi and L. Visinelli, *Hunting for extra dimensions in the shadow of M87**, *Phys. Rev. D* **100**, 024020 (2019).
- [130] Y. Chen, R. Roy, S. Vagnozzi and L. Visinelli, *Superradiant evolution of the shadow and photon ring of Sgr A**, *Phys. Rev. D* **106**, 043021 (2022).
- [131] S. Vagnozzi et al., *Horizon-scale tests of gravity theories and fundamental physics from the Event Horizon Telescope image of Sagittarius A**, arXiv:2205.07787 [gr-qc] (2022).
- [132] Y. Hou, M. Guo and B. Chen, *Revisiting the shadow of braneworld black holes*, *Phys. Rev D* **104**, 024001 (2021).
- [133] P. Li, M. Guo and B. Chen, *Shadow of a spinning black hole in an expanding universe*, *phys. Rev. D* **101**, 084041 (2020).
- [134] S. Haroon et al., *Shadow and Deflection Angle of Rotating Black Holes in Perfect Fluid Dark Matter with a Cosmological Constant*, *Phys. Rev. D* **99**, 044015 (2019).
- [135] K. Jusufi et al., *Black Hole Surrounded by a Dark Matter Halo in the M87 Galactic Center and Its Identification with Shadow Images*, *Phys. Rev. D* **100**, 044012 (2019).
- [136] X. Hou et al., *Black Hole Shadow of Sgr A* in Dark Matter Halo*, *J. Cosmol. Astropart. Phys.* **07**, 015 (2018).
- [137] R. A. Konoplya, *Shadow of a Black Hole Surrounded by Dark Matter*, *Physics Letters B* **795**, 1 (2019).
- [138] S.-W. Wei and Y.-X. Liu, *Observing the Shadow of Einstein-Maxwell-Dilaton-Axion Black Hole*, *J. Cosmol. Astropart. Phys.* **11**, 063 (2013).
- [139] B. Mashhoon, *Scattering of Electromagnetic Radiation from a Black Hole*, *Phys. Rev. D* **7**, 2807 (1973).
- [140] D. N. Page, *Particle Emission Rates from a Black Hole: Massless Particles from an Uncharged, Nonrotating Hole*, *Phys. Rev. D* **13**, 198 (1976).
- [141] L. C. B. Crispino, E. S. Oliveira, A. Higuchi, and G. E. A. Matsas, *Absorption Cross Section of Electromagnetic Waves for Schwarzschild Black Holes*, *Phys. Rev. D* **75**, 104012 (2007).
- [142] L. C. B. Crispino, A. Higuchi, and E. S. Oliveira, *Electromagnetic Absorption Cross Section of Reissner-Nordström Black Holes Revisited*, *Phys. Rev. D* **80**, 104026 (2009).
- [143] E. S. De Oliveira, *Electromagnetic Absorption, Emission and Scattering Spectra of Black Holes with Tidal Charge*, *Eur. Phys. J. Plus* **135**, 880 (2020).
- [144] A. Övgün, İ. Sakalli, J. Saavedra, and C. Leiva, *Shadow Cast of Noncommutative Black Holes in Rastall Gravity*, *Mod. Phys. Lett. A* **35**, 2050163 (2020).
- [145] R. Aldrovandi, J. G. Pereira, *Teleparallel Gravity: An Introduction. Fundamental Theories of Physics*, vol. 173 (Springer, Dordrecht, 2013).
- [146] J. W. Maluf, *The Teleparallel Equivalent of General Relativity: The Teleparallel Equivalent of General Relativity*, *Ann. Phys.* **525**, 339 (2013).
- [147] M. Krssak et al., *Teleparallel Theories of Gravity: Illuminating a Fully Invariant Approach*, *Class. Quantum Grav.* **36**, 183001 (2019).
- [148] A. Stepanian, Sh. Khlghatyan, and V. G. Gurzadyan, *Black Hole Shadow to Probe Modified Gravity*, *Eur. Phys. J. Plus* **136**, 127 (2021).
- [149] F. Kottler, *Über die physikalischen Grundlagen der Einsteinschen Gravitationstheorie*, *Ann. Phys.* **361**, 401 (1918).
- [150] Event Horizon Telescope Collaboration et al., *First Sagittarius A* Event Horizon Telescope Results. I. The Shadow of the Supermassive Black Hole in the Center of the Milky Way*, *ApJL* **930**, L12 (2022).

- [151] The Event Horizon Telescope Collaboration et al., *First M87 Event Horizon Telescope Results. I. The Shadow of the Supermassive Black Hole*, *ApJL* **875**, L1 (2019).
- [152] Planck Collaboration et al., *Planck 2018 Results: VI. Cosmological Parameters*, *A&A* **641**, A6 (2020).
- [153] S. Bahamonde et al., *Teleparallel Gravity: From Theory to Cosmology*, arXiv:2106.13793.
- [154] W. El Hanafy and G. G. L. Nashed, *Exact Teleparallel Gravity of Binary Black Holes*, *Astrophys. Space. Sci.* **361**, 68 (2016).
- [155] S. Panpanich, S. Ponglertsakul, and L. Tannukij, *Particle Motions and Gravitational Lensing in de Rham-Gabadadze-Tolley Massive Gravity Theory*, *Phys. Rev. D* **100**, 044031 (2019).
- [156] K. Nakashi et al., *Null Geodesics and Repulsive Behavior of Gravity in (2+1)D Massive Gravity*, *Prog. Theor. Exp. Phys.* **2019**, 073E02 (2019).
- [157] T. Kitamura, K. Nakajima, and H. Asada, *Demagnifying Gravitational Lenses toward Hunting a Clue of Exotic Matter and Energy*, *Phys. Rev. D* **87**, 027501 (2013).
- [158] K. Izumi et al., *Gravitational Lensing Shear by an Exotic Lens Object with Negative Convergence or Negative Mass*, *Phys. Rev. D* **88**, 024049 (2013).
- [159] T. Kitamura et al., *Microlensed Image Centroid Motions by an Exotic Lens Object with Negative Convergence or Negative Mass*, *Phys. Rev. D* **89**, 084020 (2014).
- [160] R. Shaikh and S. Kar, *Gravitational Lensing by Scalar-Tensor Wormholes and the Energy Conditions*, *Phys. Rev. D* **96**, 044037 (2017).
- [161] M. Bouhmadi-López et al., *A Consistent Model of Non-Singular Schwarzschild Black Hole in Loop Quantum Gravity and Its Quasinormal Modes*, *J. Cosmol. Astropart. Phys.* **07**, 066 (2020).
- [162] C. Gundlach, R. H. Price and J. Pullin, *Late time behavior of stellar collapse and explosions: 2. Nonlinear evolution*, *Phys. Rev. D* **49**, 890 (1994) [arXiv:gr-qc/9307010].
- [163] H. T. Cho, A. S. Cornell, J. Doukas, and W. Naylor, *Black Hole Quasinormal Modes Using the Asymptotic Iteration Method*, *Class. Quantum Grav.* **27**, 155004 (2010).
- [164] H. T. Cho, A. S. Cornell, J. Doukas, and W. Naylor, *Asymptotic Iteration Method for Spheroidal Harmonics of Higher-Dimensional Kerr-(A)DS Black Holes*, *Phys. Rev. D* **80**, 064022 (2009).
- [165] S. Ponglertsakul, T. Tangphati, and P. Burikham, *Near-Horizon Quasinormal Modes of Charged Scalar around a General Spherically Symmetric Black Hole*, *Phys. Rev. D* **99**, 084002 (2019).
- [166] S. Ponglertsakul and B. Gwak, *Massive Scalar Perturbations on Myers-Perry-de Sitter Black Holes with a Single Rotation*, *Eur. Phys. J. C* **80**, 1023 (2020).
- [167] B. F. Schutz and C. M. Will, *Black Hole Normal Modes - A Semi analytic Approach*, *The Astrophysical Journal* **291**, L33 (1985).
- [168] S. Iyer and C. M. Will, *Black-Hole Normal Modes: A WKB Approach. I. Foundations and Application of a Higher-Order WKB Analysis of Potential-Barrier Scattering*, *Phys. Rev. D* **35**, 3621 (1987).
- [169] R. A. Konoplya, *Quasinormal Behavior of the D -Dimensional Schwarzschild Black Hole and the Higher Order WKB Approach*, *Phys. Rev. D* **68**, 024018 (2003).
- [170] J. Matyjasek and M. Telecka, *Quasinormal Modes of Black Holes. II. Padé Summation of the Higher-Order WKB Terms*, *Phys. Rev. D* **100**, 124006 (2019).
- [171] V. Ferrari and L. Gualtieri, *Quasi-Normal Modes and Gravitational Wave Astronomy*, *Gen. Relativ. Gravit.* **40**, 945 (2008).
- [172] R. A. Konoplya, A. Zhidenko, and A. F. Zinhailo, *Higher Order WKB Formula for Quasinormal Modes and Grey-Body Factors: Recipes for Quick and Accurate Calculations*, *Class. Quantum Grav.* **36**, 155002 (2019).
- [173] J. P. Luminet, *Image of a spherical black hole with thin accretion disk*, *Astron. Astrophys.* **75**, 228 (1979).
- [174] Í. Güllü and A. Övgün, *Schwarzschild-like black hole with a topological defect in bumblebee gravity*, *Annals of Physics* **436**, 168721 (2022).
- [175] J. L. Synge, *The Escape of Photons from Gravitationally Intense Stars*, *Mon. Not. Roy. Astron. Soc.* **131**, no.3, 463 (1966).
- [176] V. Perlick and O. Y. Tsupko, *Calculating black hole shadows: review of analytical studies*, *Phys. Reports* **947**, 1 (2022).
- [177] R. Kumar and S. G. Ghosh, *Black Hole Parameter Estimation from Its Shadow*, *ApJ* **892**, 78 (2020).